

Stereoscopic Universal Perturbations across Different Architectures and Datasets

Zachary Berger[†]
UCLA Vision Lab

zackeberger@g.ucla.edu

Parth Agrawal[†]
UCLA Vision Lab

parthagrawal24@g.ucla.edu

Tian Yu Liu
UCLA Vision Lab

tianyu139@g.ucla.edu

Stefano Soatto
UCLA Vision Lab

soatto@cs.ucla.edu

Alex Wong
UCLA Vision Lab

alexw@cs.ucla.edu

Abstract

We study the effect of adversarial perturbations of images on deep stereo matching networks for the disparity estimation task. We present a method to craft a single set of perturbations that, when added to any stereo image pair in a dataset, can fool a stereo network to significantly alter the perceived scene geometry. Our perturbation images are “universal” in that they not only corrupt estimates of the network on the dataset they are optimized for, but also generalize to different architectures trained on different datasets. We evaluate our approach on multiple benchmark datasets where our perturbations can increase the D1-error (akin to fooling rate) of state-of-the-art stereo networks from 1% to as much as 87%. We investigate the effect of perturbations on the estimated scene geometry and identify object classes that are most vulnerable. Our analysis on the activations of registered points between left and right images led us to find architectural components that can increase robustness against adversaries. By simply designing networks with such components, one can reduce the effect of adversaries by up to 60.5%, which rivals the robustness of networks fine-tuned with costly adversarial data augmentation. Our design principle also improves their robustness against common image corruptions by an average of 70%.

1. Introduction

Deep neural networks are vulnerable to adversarial perturbations, where small changes in the input image(s) can cause large inference errors, for instance in the label of objects portrayed within. Even when the images contain sufficient information for inference, for instance in stereo where the disparity between two calibrated images is used to infer

the depth of the scene, adversarial perturbations have been shown to alter the depth map [68]. Such perturbations are ordinarily specific to each individual input, and depend on the particular deep network architecture and the particular dataset on which it is trained.

For classification, [33] showed that a single perturbation can be crafted to disrupt the inference for all images in a dataset with high probability. These are called “universal” adversarial perturbations, even though they are universal to each image in a particular dataset, and usually do not extend to different datasets. In this paper, we show the existence of stereoscopic universal perturbations (SUPs). SUPs are perturbations that can disrupt the depth or disparity estimate of different stereo networks, with different architectures, trained on different datasets, and operating on different images and domains.

Adversarial perturbations arose mainly as a means to study the topology and geometry of the decision boundary of deep networks. Since individual perturbations had to be crafted for each image, security concerns were far fetched. Universal adversarial perturbations, however, revealed vulnerabilities that could be shared among different images. Still, crafting them required knowledge of the architecture and availability of the training set. In contrast, the existence of universal adversarial perturbations for stereo and other spatial inference tasks, common in robotics and autonomy, suggests that such perturbations could present a concern, especially if they can be applied to different images, processed by different neural network models that are trained on different datasets. To the best of our knowledge, we are the first to show, for stereo, that universal perturbations can be applied effectively *even without* knowledge of the trained model, and generalize across domains and datasets. Such perturbations can be optimized on an off-the-shelf model and realized as a filter to be placed on top of a camera lens.

Our main methodological innovation is to design SUPs so that they are approximately space equivariant. We build

[†] denotes authors with equal contributions.

Code: github.com/alexklwong/stereoscopic-universal-perturbations



Figure 1. *Universality across models and datasets.* We optimized a single pair of perturbation images for AANet on the KITTI dataset. When added to a stereo pair from KITTI 2015, it corrupts the disparity estimates of AANet and PSMNet. The same perturbations can be added to stereo pairs in Flyingthings3D to fool AANet and DeepPruner.

the perturbation out of a single tile, repeated periodically. Although the tile is not constrained to have periodic boundary conditions, we notice that the model learns perturbations where boundary artifacts are not obvious, partly because the perturbation itself is designed to be small enough to be quasi-imperceptible. Our design naturally regularizes the tile with data, allowing it to generalize to different image pairs, processed with different architectures trained with different datasets – increasing error from 1% to as much as 87% when added to network inputs.

In our experiments, we observe that the errors in disparity induced by SUPs are more pronounced on certain classes of objects. We conjecture that this is due to said classes exhibiting more homogeneous regions, which are more prone to errors in disparity due to ambiguity. We also found that there is a systematic bias towards closer distance (larger disparity) after perturbations. To study the effect of SUPs on stereo networks, we investigate the activations of left and right feature maps before and after adding perturbations. We validate empirically that the embedding function amplifies the adversarial signal: The embedding of perturbed registered features between the images grows more uncorrelated throughout a forward pass than the embedding of the original or “clean” registered features, which “fools” a stereo network into estimating incorrect correspondences.

Moreover, we use SUPs to improve robustness in stereo networks. We study the effect that different architectural elements (deformable convolutions, and explicit matching modules) have on mitigating perturbations. We observe that by simply designing networks with these elements (and following standard training protocols), one can reduce the effect of adversaries to a similar degree as fine-tuning a model (that lacks such elements) with adversarial data augmentation. While robustness is increased with fine-tuning, it come at a significant cost in time and compute. In contrast, the proposed architectural design choices can mitigate attacks (60.5% error reduction), and only require a few lines of code; they also improve robustness against common im-

age perturbations i.e. lossy compression, noise, blur by an average of 70%. Conclusions are valid for three different architectures, across three datasets. While these are chosen to represent the variety in use today, we cannot exclude that there could be tasks, data and models on which our method to craft perturbations is ineffective, and conversely perturbations that are not mitigated by the methods we propose.

Our contributions include: (i) The design of the first stereoscopic universal perturbations (SUPs) that can not only fool the network they are optimized for, but also other networks across multiple datasets. We perform an empirical analysis on how SUPs affect (ii) the estimated scene geometry, (iii) different object classes, and (iv) the features of registered points in a stereo pair. Our results shed light on how SUPs fool stereo networks and led us to uncover (v) architectural designs, i.e. deformable convolution and explicit feature matching, that mitigate the effect of SUPs to a similar degree as fine-tuning on them. A discussion of potential negative societal impact is available in Supp. Mat.

2. Related Work

Adversarial perturbations. [59] showed that small additive signals can significantly alter the output of a classification network. [16] introduced the fast gradient sign method (FGSM). [11, 24, 30] extended FGSM to iterative optimization to boost its potency. [34] found the minimal perturbation to alter the predicted class while [44] computed the lower bounds on the perturbation magnitudes required to fool a network. [40] showed that unrecognizable noise can yield high confidence outputs and [22] attributed adversaries to non-robust features. [76] improved their transferability across networks with geometric image augmentations. [39] studied their transferability across datasets.

[33] proposed *universal* adversarial perturbations, where the same perturbation can be added to any image in a dataset to fool a network. [35] showed that data independent universal perturbations are transferable across different networks and [36] proposed data-free objectives for craft-

ing them. [19, 37, 48] use generative models to form universal perturbations. [51] proposed universal attacks on graphs, meshes, and point clouds. For those interested, see [6] for an extensive survey. We also study universal perturbations, but unlike past works focused on single image based problems, we consider the deep stereo matching, where the latent variable (disparity) is constrained by the stereo pair.

Efforts to defend against adversarial attack include adversarial data augmentation during training [24, 61], which can be improved with randomization [74]. [38, 57] proposed universal adversarial training, [4, 72] gradient discretization, and [42, 50, 71] randomization. [1, 18, 49, 54] performed purification, and [28] denoising to rectify the image. [73] used batch normalization to mitigate perturbations. [8] used adversarial learning to improve object detection.

Despite many works on adversarial perturbations for classification, few study dense-pixel prediction tasks e.g. segmentation, optical flow, depth estimation. [75] showed adversarial perturbations for object detection and segmentation. [20] proposed universal perturbations for segmentation, while [36] studied them for segmentation and single image depth. [64] showed targeted attacks for single image depth while [10] studied them using images augmented with synthetic vehicles. [88] examined translucent patch attacks for object detection, and [53] visible patch attacks on optical flow. [56] proposed defenses against physical attacks for optical flow. [68] demonstrated adversarial attacks for stereo. Like [68], we also consider stereo, but instead, we study universal perturbations and show that the same perturbations generalize across network architectures and datasets.

Deep Stereo Matching. Early works [82, 83] replaced hand-crafted features with deep features for more robust matching. Recent works realize the entire stereo pipeline as an inductive bias, from feature extraction to cost matching, into 2D and 3D network architectures. 2D architectures leverage correlation layers for matching. For instance, [31] formed a 2D cost volume with correlation over left and right features. [41] extended [31] to a cascade residual learning framework. AANet [77] also used correlation, but proposed deformable convolutions [85] when performing cost aggregation to avoid sampling at discontinuities. 3D architectures use feature concatenation and sparse patch matching. [23] concatenated left and right features together to build a 3D cost volume. PSMNet [5] added spatial pyramid pooling layers and introduced a stacked hourglass architecture. [84] used local and global cost aggregation. DeepPruner [12] proposed differentiable patch matching over deep features to construct their cost volume.

We demonstrate the existence of universal adversarial perturbations on PSMNet, DeepPruner and AANet. We chose them as architectural exemplars for the stereo matching task. PSMNet represents the modern stereo networks (stacked hourglass, cost volume, 3D convolutions), but uses

feature stacking without explicit matching. DeepPruner follows the architecture of PSMNet, but performs explicit matching with PatchMatch [3]. AANet represents the state of the art in 2D architecture and uses correlation.

3. Universal Perturbations for Stereo

Formulation. Let $f_\theta(x_L, x_R) \in \mathbb{R}^{H \times W}$ be a pre-trained stereo network that estimates the disparity between the left x_L and right x_R images of a stereo pair and \mathcal{X} be a distribution of stereo pairs that belongs to the set of natural images. Our goal is to craft a single pair of image-agnostic stereoscopic universal perturbation images (SUPs) $v_L, v_R \in [0, 1]^{H \times W \times 3}$ that, when added to (x_L, x_R) , corrupts the disparity estimate such that $f_\theta(x_L, x_R) \neq f_\theta(\hat{x}_L, \hat{x}_R)$ where $\hat{x}_L = x_L + v_L$ and $\hat{x}_R = x_R + v_R$ for $(x_L, x_R) \sim \mathcal{X}$. To ensure that the SUPs are small or quasi-imperceptible, we subject them to the norm constraints $\|v_I\|_\infty \leq \epsilon$ for $I \in \{L, R\}$.

We assume a dataset $X := \{(x_L^{(n)}, x_R^{(n)}, y_{gt}^{(n)})\}_{n=1}^N$ sampled from \mathcal{X} as a “training” set, and access to a stereo network f_θ and its loss function $\ell(f_\theta(\cdot), y_{gt})$ where y_{gt} denotes the ground truth. We note that, unlike classification or segmentation, it is rare for any large scale stereo dataset to provide ground truth for every sample, so instead we use disparity estimated from “clean” stereo pairs, i.e. without any perturbations, as pseudo ground truth, $y^{(n)} = f_\theta(x_L^{(n)}, x_R^{(n)})$.

Algorithm. To craft universal perturbations subject to the norm constraint of $\|v_I\|_\infty \leq \epsilon$, we propose to generate (v_L, v_R) by iterating through X and gradually aggregating small perturbation vectors that are able to fool the stereo network f_θ into altering its output disparity or the perceived scene geometry for a given image pair $(x_L^{(n)}, x_R^{(n)}) \in X$. At each iteration, we compute the gradient of the loss ℓ with respect to each image x_I in the stereo pair for $I \in \{L, R\}$:

$$g_I^{(n)} = \nabla_{x_I^{(n)}} \ell(f_\theta(\hat{x}_L^{(n)}, \hat{x}_R^{(n)}), y^{(n)}). \quad (1)$$

Then, project it onto a smaller (than ϵ) ball with radius α (akin to a learning rate) via the projection operator¹ and aggregate it to the current perturbations:

$$v_I = v_I + \mathbf{p}_{\infty, \alpha}(g_I^{(n)}). \quad (2)$$

Finally, we project v_I onto the ϵ radius ball after each iteration to ensure our perturbations meet the upper norm constraint. The procedure is repeated for all stereo pairs in X . See Alg. 1 for more details.

Towards universality across model and data. We aim to optimize a single pair of perturbations that can alter the perceived geometry of a scene, not just for the network and dataset it is optimized for, but for an array of different unseen network architectures across multiple datasets. To this

¹ $\mathbf{p}_{p, \xi}(v) = \arg \min_{v'} \|v - v'\|$ subject to $\|v'\|_p < \xi$

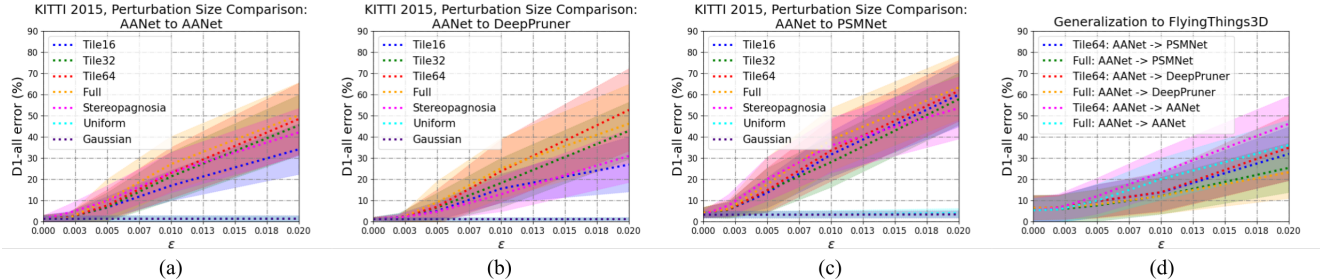


Figure 2. *The effect of perturbation size.* All methods are robust to naive attacks of uniform and Gaussian noise, as performance is constant across ϵ . Hence, we optimize a pair of perturbations on KITTI for AANet and attack (a) AANet, (b) DeepPruner, and (c) PSMNet. Amongst the perturbation sizes, full and 64×64 are the most effective at degrading performance on KITTI 2015 validation set. In (d), we show transferability to FlyingThings3D by using the same perturbations optimized on KITTI from (a)-(c) to attack models trained on Scene Flow. The 64×64 perturbations generalize the best across datasets.

Algorithm 1 Computing universal perturbations.

Parameters: Upper norm ϵ , learning rate α .
Inputs: Dataset X , pre-trained stereo network f_θ .
Outputs: Perturbations v_L, v_R .
Initialize: $v_L = \mathbf{0}, v_R = \mathbf{0}$.
for each stereo pair $(x_L^{(n)}, x_R^{(n)}) \in X$ **do**
 Compute $g_L^{(n)}$ and $g_R^{(n)}$ as defined in Eqn. 1
 $v_L = \mathbf{P}_{\infty, \epsilon}(v_L + \mathbf{P}_{\infty, \alpha}(g_L^{(n)}))$
 $v_R = \mathbf{P}_{\infty, \epsilon}(v_R + \mathbf{P}_{\infty, \alpha}(g_R^{(n)}))$
end for

end, the perturbations must be spatially invariant to generalize across different scene distributions i.e. roads are commonly at the center of the image for outdoor driving scenarios, but a variety of shapes may populate the same region for indoors. Hence, rather than optimizing (v_L, v_R) that span the full $H \times W$ image domain, we reduce (v_L, v_R) to a pair of $h \times w$ patches or tiles subject to $h \mid H$ and $w \mid W$. We note that full size $H \times W$ perturbations are a special case.

To apply (v_L, v_R) to (x_L, x_R) over the entire image space, we evenly repeat or tile the perturbation v_I across x_I with no overlap. Formally, we let $x_I(i, j)$ be the $h \times w$ image region that spans from pixel position (i, j) to $(i + h, j + w)$ for $i \in \{0, \frac{H}{h}, \dots, \frac{H(h-1)}{h}\}$ and $j \in \{0, \frac{W}{w}, \dots, \frac{W(w-1)}{w}\}$. Thus, the perturbed image region is:

$$\hat{x}_I(i, j) = x_I(i, j) + v_I \quad \forall i, j. \quad (3)$$

We now modify the the gradient computation step in Alg. 1 for a given stereo pair $(x_L^{(n)}, x_R^{(n)})$ by taking the mean over the gradient with respect to the image $g_I^{(n)}$ for all tiles

$$\bar{g}_I^{(n)} = \frac{h \cdot w}{H \cdot W} \sum_{i, j} g_I^{(n)}(i, j). \quad (4)$$

In doing so, we prevent the perturbations from overfitting to the bias in scene structures induced by the training set e.g. road on bottom of the image and sky on top. We demonstrate in Sec. 4 that this approach yields a single set of universal perturbations that can fool different models across

multiple datasets. We note that we can extend our approach to patch attacks by adding the perturbations anywhere on the image, instead of tiling across the image. However, because we constrain our perturbations to be within a small ϵ ball, unlike [53], a visually imperceptible patch attack is limited in its effect on fooling the network.

4. Experiments and Results

We optimized our SUPs on the KITTI raw dataset [14] and evaluated them on KITTI 2012, KITTI 2015 [32] for stereo models [5, 12, 77]. We also show that the same SUPs generalize to FlyingThings3D [31] to disrupt models trained on Scene Flow [31]. Please see Supp. Mat. for details on datasets, hyper-parameters and implementation.

On the effect of perturbation size. We optimize SUPs on AANet using square tiles of 16, 32, and 64, and the full image size of 256×640 . We report results in Fig. 2, which shows the performance of each network on KITTI 2015 when attacked by these perturbations. We compare our results against [68] which uses image-specific perturbations generated with FGSM. We additionally consider two naive attacks that perturb the input stereo pair (x_L, x_R) with uniform $\mathcal{U}(-\epsilon, \epsilon)$ and Gaussian $\mathcal{N}(0, (\epsilon/4)^2)$ noise.

Fig. 2-(a, b, c) show that naive attacks have little effect on stereo networks, as the D1-error is roughly constant for all ϵ . Hence, stereo networks are robust to naive perturbations within ϵ upper norm, and fooling them is non-trivial. Among all square tiles, 64×64 causes the largest error for all networks across all ϵ . We note that, although our SUPs are image-agnostic, we are comparable to [68] on small norms and beat them on larger norms. Fig. 3 shows the 64×64 tiles optimized on KITTI for AANet, DeepPruner, and PSMNet. When added to a stereo pair from KITTI 2015, the disparity estimated by each network is corrupted.

For FlyingThings3D, we consider the full and 64×64 SUPs (both trained on KITTI) as they caused the most corruption on KITTI 2015. Fig. 2-(d) shows that 64×64 generalizes better than full-size SUPs across networks. For $\epsilon = 0.02$, 64×64 achieves 46.14% error on AANet, 34.87%

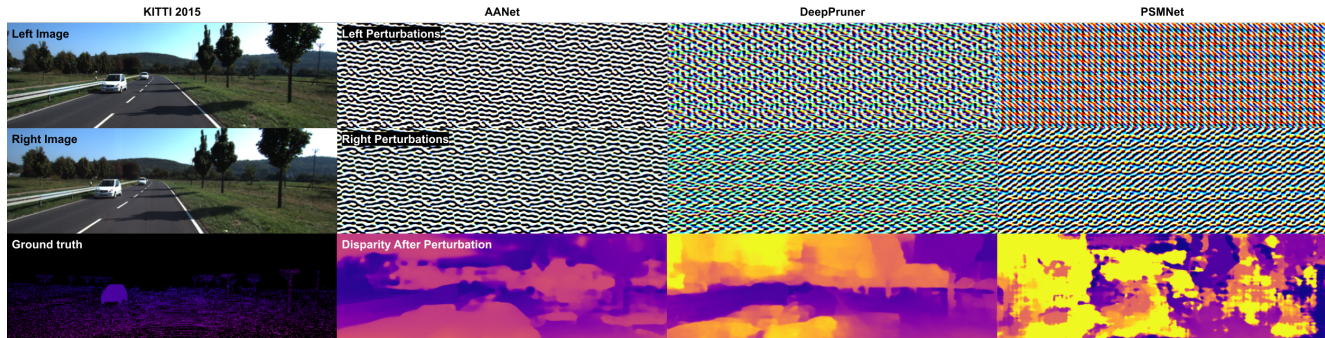


Figure 3. *Attacking stereo networks.* We visualize 64×64 perturbations (tiled across the image domain) optimized for AANet, DeepPruner, and PSMNet on the KITTI dataset. When added to the inputs of the network for which they were optimized, the perturbations can corrupt the estimated disparities. Note: the damage is concentrated on textureless regions e.g. sky, road.

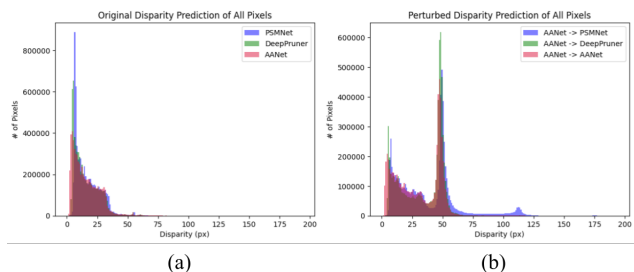


Figure 4. *Distribution of disparities before and after adding perturbations.* (a) Before adding perturbations, most of the scene is estimated to be ≈ 2 disparities. (b) The perturbations fool the networks into predicting larger (≈ 50) disparities.

on DeepPruner and 31.93% on PSMNet, while full achieves 36.09%, 23.28%, and 25.35%, respectively. Thus, our tiling approach can help generalize to different data distributions. As our goal is universality across architectures and datasets, we use 64×64 perturbations for the rest of our experiments.

Generalization across architectures and datasets. We optimized three sets of 64×64 SUPs on KITTI for AANet, DeepPruner, and PSMNet, respectively. In Fig. 5, we attack each network with each set of SUPs on three datasets. We report D1-error for KITTI 2012, and 2015, and EPE for FlyingThings3D (see Supp. Mat. for results for KITTI 2012). For KITTI 2015, Fig. 5-(a) shows that, when trained on the network to be attacked, SUPs with $\epsilon = 0.02$ cause error to rise from 1.47% to 48.43% for AANet, 1.28% to 52.74% for DeepPruner, and 4.25% to 87.72% for PSMNet. While SUPs with $\epsilon = 0.002$ have negligible impact, relaxing ϵ to 0.005 increases the error of AANet to 7.62%, DeepPruner to 8.90%, and PSMNet to 28.97%. Fig. 5-(b) shows that SUPs generalize to other data distributions as well. Adding SUPs optimized on KITTI to FlyingThings3D causes increases in EPE for models trained on Scene Flow – from 1.30px to 9.47px for AANet, 1.25px to 14.77px for DeepPruner, and 1.27px to 18.88px for PSMNet.

For all three datasets, our SUPs also generalize across architectures. For example, SUPs with $\epsilon = 0.02$ optimized for AANet on KITTI can be added to stereo pairs in

KITTI 2015 to fool DeepPruner (from 1.28% to 52.66%), and PSMNet (from 4.25% to 61.66%). Similarly, the same SUPs can be added to images in FlyingThings3D to corrupt the outputs of PSMNet (from 1.27 to 6.86px) and DeepPruner (1.25 to 6.60px). Yet, transferability is not symmetric e.g. SUPs optimized for DeepPruner on KITTI only corrupt AANet predictions from 1.30 to 4.49px on Flyingthings3D. Fig. 8 demonstrates the transferability qualitatively, showing corruption against PSMNet on FlyingThings3D.

In our experiments, we found AANet to be the most robust and PSMNet the least. We hypothesize that explicit matching plays a role because DeepPruner shares the same architecture as PSMNet, with the exception of a PatchMatch module, but is significantly more robust. Like DeepPruner, AANet also employs matching, but replaces convolutions with deformable convolutions – we explore the use of these architectural designs as a defense in Sec. 5.

Effect on scene geometry. To quantify how SUPs affect the estimated scene geometry, we compare the disparities estimated for “clean” (no added perturbations, Fig. 4-(a)) and perturbed (optimized on AANet, Fig. 4-(b)) stereo pairs. Fig. 4 shows that the peak of the distribution shifts from ≈ 2 to ≈ 50 px for all three networks. For PSMNet, we see an additional mode at ≈ 110 px. Depth and disparity are inversely related, so the SUPs fool the network to predict the scene to be closer to the camera. We observe similar trends for DeepPruner and PSMNet (see Supp. Mat.).

Robustness of semantic classes. To analyze their effect on objects populating the scene, we use SDCNet [87] to obtain segmentation maps for the KITTI 2015 validation set. We measure the per class error and found that different semantic classes exhibit different levels of robustness against adversaries. Specifically, Fig. 6 shows that *sky* and *vegetation* are the least robust with 72.96% and 58.52% D1-error, respectively; whereas, *truck* (14.19%) and *car* (16.82%) are the most robust. We observe that the least robust classes are largely homogeneous. We conjecture that these regions are most vulnerable because locally they give little to no information about scene structure, which leads to ambigu-

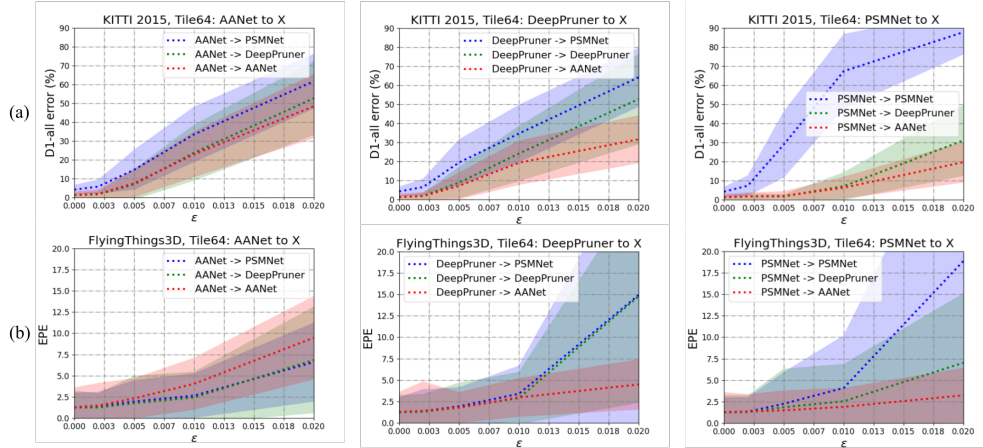


Figure 5. *Generalization across architectures and datasets.* Perturbations were optimized for AANet, DeepPruner, and PSMNet on KITTI and added to stereo pairs of KITTI 2015, and FlyingThings3D. Despite being optimized for a specific model on KITTI, they can corrupt models trained on KITTI for KITTI 2015 and those trained on Scene Flow for FlyingThings3D.

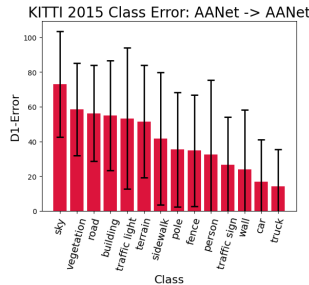


Figure 6. *D1-error for each semantic class for perturbed images.* Each class exhibit different levels of robustness. Homogeneous regions (sky, vegetation) are most vulnerable.

ity when registering points between two images – this is in contrast to sufficiently textured regions where unique correspondences are to be found. Thus, the network must rely on the regularizer (stored in the weights) learned from the training set to fill in the disparity for homogeneous regions.

Effect on feature maps. As DeepPruner and AANet use explicit matching to form their cost volume, there is a well-defined measure of data-fidelity to register the left and right images. So, to alter disparity, SUPs must corrupt the features used in the matching process. Hence, to quantify their effect, we measure the correlation between left and right feature maps before and after perturbing the images.

Let $f_{\theta}^{(l)}$ be the l -th layer of the encoder shared between the stereo pair and $u \in \Omega$, the image domain. To quantify how SUPs corrupt the feature maps, we compute the correlation between $f_{\theta}^{(l)}(x_L(u))$ and $f_{\theta}^{(l)}(\hat{x}_L(u))$ for all l . Fig. 7-(a, b) shows that when SUPs optimized for AANet are added to the input, the correlation between clean and perturbed left and right features grow uncorrelated from 1 to 0.76 during a forward pass i.e. the embedding function amplifies the effect of perturbation. We observe similar trends for DeepPruner and PSMNet (see Supp. Mat.).

While the observations in Fig. 7-(a, b) may be suffi-

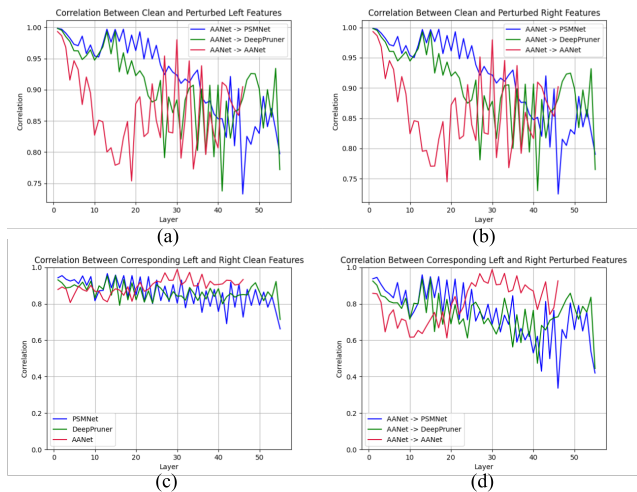


Figure 7. *Effect on features.* Clean and perturbed left (a) and right (b) features grow uncorrelated. Features of clean stereo pairs are correlated (c), but after perturbation, become uncorrelated (d).

cient to fool a classification network, i.e. the feature maps are transformed across a decision boundary, it is not sufficient for stereo matching. To fool a stereo network, SUPs must alter the correspondences between left and right image. In other words, for a pair of registered points $x_L(u)$ and $x_R(u - y_{gt}(u))$, where $y_{gt} \in \mathbb{R}^{H \times W}$ is the true disparity, the perturbations must cause the features of these similar points in the image to be dissimilar in embedding space. To quantify this, we first compute the correlation between the registered clean stereo pair $f_{\theta}^{(l)}(x_L(u))$ and $f_{\theta}^{(l)}(x_R(u - y_{gt}(u)))$ in Fig. 7-(c). As expected the feature maps of the registered points are well correlated. In Fig. 7-(d), we compute the correlation between the registered perturbed stereo pair $f_{\theta}^{(l)}(\hat{x}_L(u))$ and $f_{\theta}^{(l)}(\hat{x}_R(u - y_{gt}(u)))$. Indeed, the registered perturbed feature maps grow uncorrelated relative to the clean feature maps in the forward pass i.e. the perturbations cause similar regions in the RGB do-

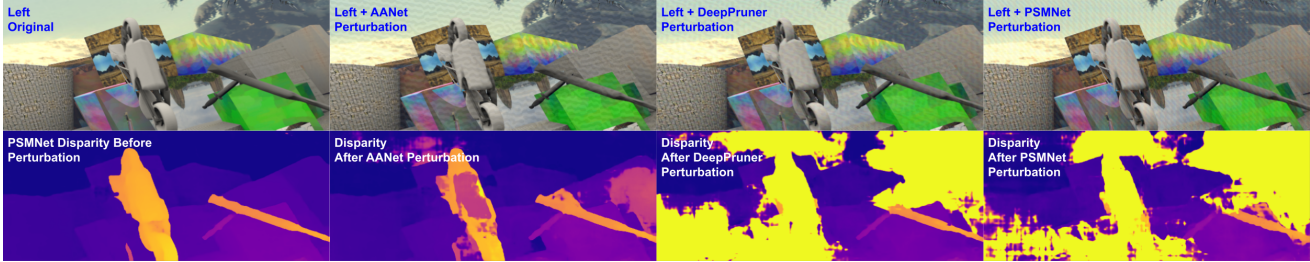


Figure 8. *Transferability to PSMNet*. Stereoscopic universal perturbations optimized on KITTI for AANet, DeepPruner, and PSMNet can generalize to stereo pairs in FlyingThings3D to corrupt the disparity estimation of PSMNet.

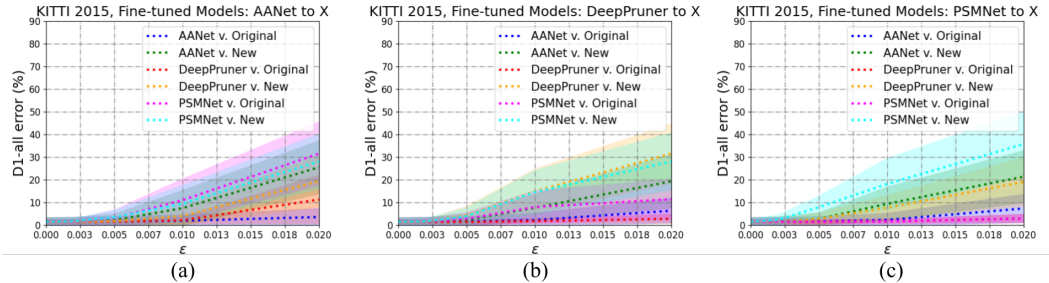


Figure 9. *Adversarial data augmentation*. AANet, DeepPruner, and PSMNet were fine-tuned with adversarial data augmentation. Each model was attacked with a perturbation trained for the original and fine-tuned AANet (a), DeepPruner (b), and PSMNet (c). Fine-tuning with adversarial data augmentation is an effective defense against SUPs trained for the original model, but does not fully mitigate a new adversary. Fine-tuning a model on SUPs optimized for it increases robustness against perturbations optimized for different architectures.

main to be dissimilar in the embedding space, resulting in incorrect points being matched. Note that, like in Fig. 7-(a) and Fig. 7-(b), correlation between left and right AANet features increases from layer 20 to 30; this coincides with deformable convolutions. We conjecture that this may be related to AANet’s relative robustness against adversaries.

5. Towards Robust Deep Stereo Networks

Adversarial data augmentation. As shown in [68], fine-tuning with adversarial data augmentation is among the best performing defenses for stereo. Hence, we first fine-tuned each pretrained stereo model on KITTI 2015 with SUPs of $\epsilon \in \{0.002, 0.005, 0.01, 0.02\}$ trained for the model. The SUPs were randomly added the inputs with 50% probability. In Fig. 9, we attack each fine-tuned model with a perturbation trained for the original and fine-tuned variant of each architecture. Fig. 9 shows that adversarial data augmentation improves the robustness of each model. When attacked by the SUPs it is fine-tuned on, AANet reduces in error from 48.43% to 3.62%, DeepPruner from 52.74% to 2.83%, and PSMNet from 87.72% to 2.96% for $\epsilon = 0.02$. New adversaries optimized for the fine-tuned networks are less effective, with AANet dropping to 25.54% error, DeepPruner to 31.54%, and PSMNet to 35.75%.

Fig. 9 also shows that fine-tuning a model on SUPs optimized for it increases robustness against SUPs optimized for different architectures. For example, Fig. 9-(a) shows that fine-tuning reduces AANet in error from 48.43% to 3.62%, DeepPruner from 52.74% to 11.32%, and PSMNet

from 87.72% to 31.54% when attacked by SUPs optimized for the original AANet with $\epsilon = 0.02$. Note that AANet has the lowest error against the original AANet adversary because it was fine-tuned on that perturbation, whereas DeepPruner and PSMNet are seeing it as a “new” adversary. Similar results are shown for SUPs optimized for DeepPruner (Fig. 9-(b)) and PSMNet (Fig. 9-(c)). We note that this process of optimizing SUPs and fine-tuning on them is time consuming, and the resulting networks are not fully robust.

On explicit matching (EM) and deformable convolution (DC). Instead, we propose to make simple modifications to the design of stereo networks. From our observations, EM increases robustness as PSMNet (no explicit matching) is more vulnerable than AANet and DeepPruner. Fig. 7 shows that the effect of SUPs is amplified by the embedding function, which ultimately fools the network; we conjecture that EM mitigates this by explicitly registering correspondences based on similarity rather than propagating the local signal. This intuition extends to DCs that learn convolutional offsets to regions locally similar to the element being convolved over and in effect “avoids” the adversarial signal – Fig. 7 shows an increase in AANet’s feature correlation that coincides with DCs. While the intent of DC is to minimize artifacts e.g. over-smoothing along occlusion boundaries by sampling features that are robust to local deformation and respect boundary conditions, we hypothesize that this filters out the perturbation signal that causes dissimilarities within a patch, and is the reason DC (and EM) allows AANet to be more robust.

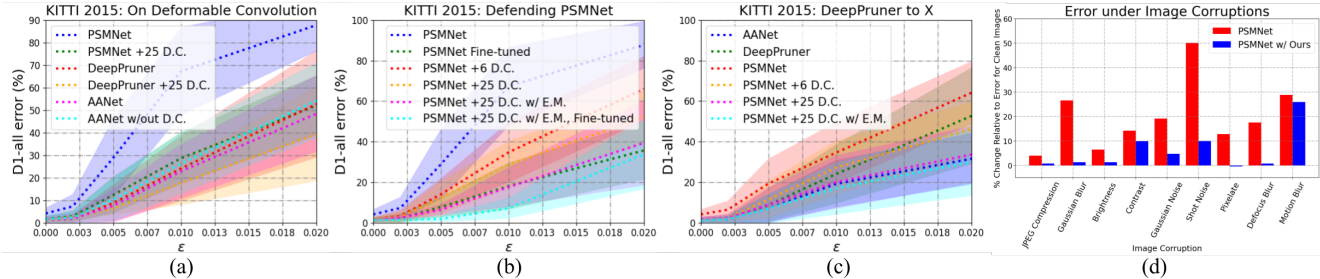


Figure 10. *Improving robustness against perturbations.* In (a, b), each variant was attacked by perturbations optimized specifically for them on image pairs. (a) Adding deformable convolution (DC) to PSMNet and DeepPruner improves their robustness, while removing it from AANet decreases its robustness. The least robust model, PSMNet, can achieve comparable performance to the most robust model, AANet, when using DC and explicit matching (EM). (b) Adding DC and EM to PSMNet achieves comparable results to adversarial training. (c) PSMNet with DC and EM is more robust than AANet under black-box attack, where the adversary was optimized for a different model (DeepPruner). (d) By applying our design principles to PSMNet, we improve its robustness to common image corruptions by $\approx 70\%$.

To assess DC as an inherent defense against adversarial perturbations, we trained (i) PSMNet and (ii) DeepPruner, each with 25 DCs, and (iii) AANet without DCs. We optimized six pairs of SUPs on KITTI for vanilla AANet, DeepPruner, PSMNet, and their variants. In Fig. 10-(a), we show results on KITTI 2015, where each network was attacked by SUPs optimized specifically for them. We found that DCs do improve robustness as both DeepPruner and PSMNet produced lower D1-errors across all norms. For $\epsilon = 0.02$, DeepPruner drops in error from 52.74% to 39.47%, and PSMNet drops from 87.72% to 52.10%. Conversely, replacing DCs with regular convolutions can make a model more susceptible to adversaries – AANet without DCs is less robust, as D1-error increase from 48.43% to 54.32%. In summary, simply designing a network with DC, the least robust model, PSMNet, can become comparable in performance to AANet, the most robust model.

Next, we assessed how EM and DC compare to adversarial training. We trained variants of PSMNet with (i) 6 DCs, (ii) 25 DCs, and (iii) 25 DCs and EM i.e. DeepPruner with 25 DCs. We performed adversarial fine-tuning on PSMNet and (iii). In Fig. 10-(b), we observe for $\epsilon = 0.02$ that increasing the number of DCs and then adding explicit matching drops the D1-error of PSMNet from 87.72% to 66.10%, 52.10%, and finally to 39.47%. PSMNet fine-tuned on SUPs also performs well; however, with a D1-error of 35.75%, it only marginally beats PSMNet with 25 DCs and explicit matching on $\epsilon = 0.02$. For all other norms, the two are comparable. The best performing variant is PSMNet with DCs and EM fine-tuned on SUPs, achieving D1-error of 33.85%. So, simply using DCs and EM and following standard training protocols can yield more robust networks with no explicit intent for defense. Moreover, they can also be used in conjunction with existing defenses (i.e. adversarial fine-tuning) to yield even more robust networks.

In Fig. 10-(c), we simulate the realistic black-box scenario where an attacker does not have access to a network (PSMNet or AANet) and crafts SUPs with an off-the-shelf

model (DeepPruner). Replacing convolutions in PSMNet with DCs leads to immediate improvements in robustness with no loss in accuracy on clean images. With just 6 DCs, PSMNet becomes more robust than DeepPruner and with 25 it is on par with AANet. Incorporating PatchMatch into PSMNet (i.e. DeepPruner) with 25 DCs improves it to the most robust method. Note: fine-tuning on SUPs as data augmentation can further improve its robustness (Fig. 10-(b)).

Designing networks with DCs and inductive biases like EM not only improves robustness against SUPs, but also against common image corruptions i.e. lossy compression, blur and noise. Fig. 10-(d) shows that PSMNet (red) is susceptible to blurring and shot noise where the latter can increase error by 50%. Our design improves its robustness across all common corruption. Particularly, Gaussian and defocus blur, and pixelation have little effect – we improve by as much as 80% on shot noise and 70% on average.

6. Discussion

Stereoscopic universal perturbations (SUPs) exist and can generalize across architectures and datasets. SUPs can be partly mitigated by fine-tuning with adversarial data augmentation. However, doing so is costly in time and compute. Instead, we propose to address the robustness problem starting from the the design of deep networks. We have identified architectural elements, i.e. deformable convolutions and explicit matching, which can be easily incorporated into stereo networks with few lines of code and trained with standard protocol. The resulting networks are comparable in robustness and performance to those without these elements, but fine-tuned on adversarial examples. Admittedly, SUPs do not exist in nature; nonetheless, our design is also applicable to common image corruptions. While the our scope is limited to stereo, many geometry problems i.e. optical flow share similar architectural designs. So we hope this work can contribute to robust systems in related fields.

Acknowledgements. We thank ARL W911NF-20-1-0158, ONR N00014-19-1-2229 and ARO W911NF-17-1-0304.

References

- [1] Naveed Akhtar, Jian Liu, and Ajmal Mian. Defense against universal adversarial perturbations. In *Proceedings of the IEEE Conference on Computer Vision and Pattern Recognition*, pages 3389–3398, 2018. 3
- [2] Filippo Aleotti, Matteo Poggi, Fabio Tosi, and Stefano Mattoccia. Learning end-to-end scene flow by distilling single tasks knowledge. In *Proceedings of the AAAI Conference on Artificial Intelligence*, volume 34, pages 10435–10442, 2020. 21
- [3] Connelly Barnes, Eli Shechtman, Adam Finkelstein, and Dan B Goldman. Patchmatch: A randomized correspondence algorithm for structural image editing. *ACM Trans. Graph.*, 28(3):24, 2009. 3
- [4] Jacob Buckman, Aurko Roy, Colin Raffel, and Ian Goodfellow. Thermometer encoding: One hot way to resist adversarial examples. In *International Conference on Learning Representations*, 2018. 3
- [5] Jia-Ren Chang and Yong-Sheng Chen. Pyramid stereo matching network. In *Proceedings of the IEEE Conference on Computer Vision and Pattern Recognition*, pages 5410–5418, 2018. 3, 4, 13, 20, 21
- [6] Ashutosh Chaubey, Nikhil Agrawal, Kavya Barnwal, Keerat K Guliani, and Pramod Mehta. Universal adversarial perturbations: A survey. *arXiv preprint arXiv:2005.08087*, 2020. 3
- [7] Rui Chen, Songfang Han, Jing Xu, and Hao Su. Point-based multi-view stereo network. In *Proceedings of the IEEE/CVF International Conference on Computer Vision*, pages 1538–1547, 2019. 21
- [8] Xiangning Chen, Cihang Xie, Mingxing Tan, Li Zhang, Chou-Jui Hsieh, and Boqing Gong. Robust and accurate object detection via adversarial learning. In *Proceedings of the IEEE/CVF Conference on Computer Vision and Pattern Recognition*, pages 16622–16631, 2021. 3
- [9] Jifeng Dai, Haozhi Qi, Yuwen Xiong, Yi Li, Guodong Zhang, Han Hu, and Yichen Wei. Deformable convolutional networks. In *Proceedings of the IEEE international conference on computer vision*, pages 764–773, 2017. 20
- [10] Tom van Dijk and Guido de Croon. How do neural networks see depth in single images? In *Proceedings of the IEEE International Conference on Computer Vision*, pages 2183–2191, 2019. 3
- [11] Yinpeng Dong, Fangzhou Liao, Tianyu Pang, Hang Su, Jun Zhu, Xiaolin Hu, and Jianguo Li. Boosting adversarial attacks with momentum. In *Proceedings of the IEEE conference on computer vision and pattern recognition*, pages 9185–9193, 2018. 2
- [12] Shivam Duggal, Shenlong Wang, Wei-Chiu Ma, Rui Hu, and Raquel Urtasun. Deeppruner: Learning efficient stereo matching via differentiable patchmatch. In *Proceedings of the IEEE International Conference on Computer Vision*, pages 4384–4393, 2019. 3, 4, 13, 20, 21
- [13] Xiaohan Fei, Alex Wong, and Stefano Soatto. Geosupervised visual depth prediction. *IEEE Robotics and Automation Letters*, 4(2):1661–1668, 2019. 21
- [14] Andreas Geiger, Philip Lenz, and Raquel Urtasun. Are we ready for autonomous driving? the kitti vision benchmark suite. In *2012 IEEE Conference on Computer Vision and Pattern Recognition*, pages 3354–3361. IEEE, 2012. 4, 13
- [15] Clément Godard, Oisín Mac Aodha, Michael Firman, and Gabriel J Brostow. Digging into self-supervised monocular depth estimation. In *Proceedings of the IEEE/CVF International Conference on Computer Vision*, 2019. 21
- [16] Ian J Goodfellow, Jonathon Shlens, and Christian Szegedy. Explaining and harnessing adversarial examples. *arXiv preprint arXiv:1412.6572*, 2014. 2, 13
- [17] Xiaodong Gu, Zhiwen Fan, Siyu Zhu, Zuoqun Dai, Feitong Tan, and Ping Tan. Cascade cost volume for high-resolution multi-view stereo and stereo matching. In *Proceedings of the IEEE/CVF Conference on Computer Vision and Pattern Recognition*, pages 2495–2504, 2020. 21
- [18] Chuan Guo, Mayank Rana, Moustapha Cisse, and Laurens Van Der Maaten. Countering adversarial images using input transformations. *arXiv preprint arXiv:1711.00117*, 2017. 3
- [19] Jamie Hayes and George Danezis. Learning universal adversarial perturbations with generative models. In *2018 IEEE Security and Privacy Workshops (SPW)*, pages 43–49. IEEE, 2018. 3
- [20] Jan Hendrik Metzen, Mummadi Chaithanya Kumar, Thomas Brox, and Volker Fischer. Universal adversarial perturbations against semantic image segmentation. In *Proceedings of the IEEE International Conference on Computer Vision*, pages 2755–2764, 2017. 3
- [21] Mu Hu, Shuling Wang, Bin Li, Shiyu Ning, Li Fan, and Xiaojin Gong. Penet: Towards precise and efficient image guided depth completion. *arXiv preprint arXiv:2103.00783*, 2021. 21
- [22] Andrew Ilyas, Shibani Santurkar, Dimitris Tsipras, Logan Engstrom, Brandon Tran, and Aleksander Madry. Adversarial examples are not bugs, they are features. In *Advances in Neural Information Processing Systems*, pages 125–136, 2019. 2
- [23] Alex Kendall, Hayk Martirosyan, Saumitro Dasgupta, Peter Henry, Ryan Kennedy, Abraham Bachrach, and Adam Bry. End-to-end learning of geometry and context for deep stereo regression. In *Proceedings of the IEEE International Conference on Computer Vision*, pages 66–75, 2017. 3
- [24] Alexey Kurakin, Ian Goodfellow, and Samy Bengio. Adversarial machine learning at scale. *arXiv preprint arXiv:1611.01236*, 2016. 2, 3
- [25] Dong Lao and Ganesh Sundaramoorthi. Minimum delay moving object detection. In *Proceedings of the IEEE Conference on Computer Vision and Pattern Recognition*, pages 4250–4259, 2017. 21
- [26] Dong Lao and Ganesh Sundaramoorthi. Extending layered models to 3d motion. In *Proceedings of the European conference on computer vision (ECCV)*, pages 435–451, 2018. 21
- [27] Dong Lao and Ganesh Sundaramoorthi. Minimum delay object detection from video. In *Proceedings of the IEEE/CVF International Conference on Computer Vision*, pages 5097–5106, 2019. 21

- [28] Fangzhou Liao, Ming Liang, Yinpeng Dong, Tianyu Pang, Xiaolin Hu, and Jun Zhu. Defense against adversarial attacks using high-level representation guided denoiser. In *Proceedings of the IEEE Conference on Computer Vision and Pattern Recognition*, pages 1778–1787, 2018. 3
- [29] Yuankai Lin, Tao Cheng, Qi Zhong, Wending Zhou, and Hua Yang. Dynamic spatial propagation network for depth completion. *arXiv preprint arXiv:2202.09769*, 2022. 21
- [30] Aleksander Madry, Aleksandar Makelov, Ludwig Schmidt, Dimitris Tsipras, and Adrian Vladu. Towards deep learning models resistant to adversarial attacks. *arXiv preprint arXiv:1706.06083*, 2017. 2
- [31] Nikolaus Mayer, Eddy Ilg, Philip Hausser, Philipp Fischer, Daniel Cremers, Alexey Dosovitskiy, and Thomas Brox. A large dataset to train convolutional networks for disparity, optical flow, and scene flow estimation. In *Proceedings of the IEEE conference on computer vision and pattern recognition*, pages 4040–4048, 2016. 3, 4, 13
- [32] Moritz Menze and Andreas Geiger. Object scene flow for autonomous vehicles. In *Proceedings of the IEEE conference on computer vision and pattern recognition*, pages 3061–3070, 2015. 4, 13, 20
- [33] Seyed-Mohsen Moosavi-Dezfooli, Alhussein Fawzi, Omar Fawzi, and Pascal Frossard. Universal adversarial perturbations. In *Proceedings of the IEEE conference on computer vision and pattern recognition*, pages 1765–1773, 2017. 1, 2
- [34] Seyed-Mohsen Moosavi-Dezfooli, Alhussein Fawzi, and Pascal Frossard. Deepfool: a simple and accurate method to fool deep neural networks. In *Proceedings of the IEEE conference on computer vision and pattern recognition*, pages 2574–2582, 2016. 2
- [35] KR Mopuri, U Garg, and R Venkatesh Babu. Fast feature fool: A data independent approach to universal adversarial perturbations. In *British Machine Vision Conference 2017, BMVC 2017*. BMVA Press, 2017. 2
- [36] Konda Reddy Mopuri, Aditya Ganeshan, and R Venkatesh Babu. Generalizable data-free objective for crafting universal adversarial perturbations. *IEEE transactions on pattern analysis and machine intelligence*, 41(10):2452–2465, 2018. 2, 3
- [37] Konda Reddy Mopuri, Utkarsh Ojha, Utsav Garg, and R Venkatesh Babu. Nag: Network for adversary generation. In *Proceedings of the IEEE Conference on Computer Vision and Pattern Recognition*, pages 742–751, 2018. 3
- [38] Chaithanya Kumar Mummadi, Thomas Brox, and Jan Hendrik Metzen. Defending against universal perturbations with shared adversarial training. In *Proceedings of the IEEE/CVF International Conference on Computer Vision*, pages 4928–4937, 2019. 3
- [39] Muhammad Muzammal Naseer, Salman H Khan, Muhammad Haris Khan, Fahad Shahbaz Khan, and Fatih Porikli. Cross-domain transferability of adversarial perturbations. In *Advances in Neural Information Processing Systems*, pages 12905–12915, 2019. 2
- [40] Anh Nguyen, Jason Yosinski, and Jeff Clune. Deep neural networks are easily fooled: High confidence predictions for unrecognizable images. In *Proceedings of the IEEE conference on computer vision and pattern recognition*, pages 427–436, 2015. 2
- [41] Jiahao Pang, Wenxiu Sun, Jimmy SJ Ren, Chengxi Yang, and Qiong Yan. Cascade residual learning: A two-stage convolutional neural network for stereo matching. In *Proceedings of the IEEE International Conference on Computer Vision Workshops*, pages 887–895, 2017. 3
- [42] Tianyu Pang, Kun Xu, and Jun Zhu. Mixup inference: Better exploiting mixup to defend adversarial attacks. *arXiv preprint arXiv:1909.11515*, 2019. 3
- [43] Jinsun Park, Kyungdon Joo, Zhe Hu, Chi-Kuei Liu, and In-So Kweon. Non-local spatial propagation network for depth completion. In *European Conference on Computer Vision, ECCV 2020*. European Conference on Computer Vision, 2020. 21
- [44] Jonathan Peck, Joris Roels, Bart Goossens, and Yvan Saeyns. Lower bounds on the robustness to adversarial perturbations. In *Advances in Neural Information Processing Systems*, pages 804–813, 2017. 2
- [45] Matteo Poggi, Filippo Aleotti, Fabio Tosi, and Stefano Mattoccia. On the uncertainty of self-supervised monocular depth estimation. In *Proceedings of the IEEE/CVF Conference on Computer Vision and Pattern Recognition*, pages 3227–3237, 2020. 21
- [46] Matteo Poggi, Filippo Aleotti, Fabio Tosi, Giulio Zaccaroni, and Stefano Mattoccia. Self-adapting confidence estimation for stereo. In *European Conference on Computer Vision*, pages 715–733. Springer, 2020. 21
- [47] Matteo Poggi, Fabio Tosi, Filippo Aleotti, and Stefano Mattoccia. Real-time self-supervised monocular depth estimation without gpu. *IEEE Transactions on Intelligent Transportation Systems*, 2022. 21
- [48] Omid Poursaeed, Isay Katsman, Bicheng Gao, and Serge Belongie. Generative adversarial perturbations. In *Proceedings of the IEEE Conference on Computer Vision and Pattern Recognition*, pages 4422–4431, 2018. 3
- [49] Aaditya Prakash, Nick Moran, Solomon Garber, Antonella DiLillo, and James Storer. Deflecting adversarial attacks with pixel deflection. In *Proceedings of the IEEE conference on computer vision and pattern recognition*, pages 8571–8580, 2018. 3
- [50] Edward Raff, Jared Sylvester, Steven Forsyth, and Mark McLean. Barrage of random transforms for adversarially robust defense. In *Proceedings of the IEEE/CVF Conference on Computer Vision and Pattern Recognition*, pages 6528–6537, 2019. 3
- [51] Arianna Rampini, Franco Pestarini, Luca Cosmo, Simone Melzi, and Emanuele Rodola. Universal spectral adversarial attacks for deformable shapes. In *Proceedings of the IEEE/CVF Conference on Computer Vision and Pattern Recognition*, pages 3216–3226, 2021. 3
- [52] René Ranftl, Alexey Bochkovskiy, and Vladlen Koltun. Vision transformers for dense prediction. In *Proceedings of the IEEE/CVF International Conference on Computer Vision*, pages 12179–12188, 2021. 21
- [53] Anurag Ranjan, Joel Janai, Andreas Geiger, and Michael J Black. Attacking optical flow. In *Proceedings of the IEEE*

- International Conference on Computer Vision*, pages 2404–2413, 2019. [3](#), [4](#)
- [54] Pouya Samangouei, Maya Kabkab, and Rama Chelappa. Defense-gan: Protecting classifiers against adversarial attacks using generative models. *arXiv preprint arXiv:1805.06605*, 2018. [3](#)
- [55] Daniel Scharstein and Richard Szeliski. A taxonomy and evaluation of dense two-frame stereo correspondence algorithms. *International journal of computer vision*, 47(1):7–42, 2002. [20](#)
- [56] Simon Schrodi, Tonmoy Saikia, and Thomas Brox. What causes optical flow networks to be vulnerable to physical adversarial attacks. *arXiv preprint arXiv:2103.16255*, 2021. [3](#)
- [57] Ali Shafahi, Mahyar Najibi, Zheng Xu, John Dickerson, Larry S Davis, and Tom Goldstein. Universal adversarial training. In *Proceedings of the AAAI Conference on Artificial Intelligence*, volume 34, pages 5636–5643, 2020. [3](#)
- [58] Deqing Sun, Xiaodong Yang, Ming-Yu Liu, and Jan Kautz. Pwc-net: Cnns for optical flow using pyramid, warping, and cost volume. In *Proceedings of the IEEE conference on computer vision and pattern recognition*, pages 8934–8943, 2018. [21](#)
- [59] Christian Szegedy, Wojciech Zaremba, Ilya Sutskever, Joan Bruna, Dumitru Erhan, Ian Goodfellow, and Rob Fergus. Intriguing properties of neural networks. *arXiv preprint arXiv:1312.6199*, 2013. [2](#), [13](#)
- [60] Zachary Teed and Jia Deng. Raft: Recurrent all-pairs field transforms for optical flow. In *European conference on computer vision*, pages 402–419. Springer, 2020. [21](#)
- [61] Florian Tramèr, Alexey Kurakin, Nicolas Papernot, Ian Goodfellow, Dan Boneh, and Patrick McDaniel. Ensemble adversarial training: Attacks and defenses. *arXiv preprint arXiv:1705.07204*, 2017. [3](#)
- [62] Fangjinhua Wang, Silvano Galliani, Christoph Vogel, Pablo Speciale, and Marc Pollefeys. Patchmatchnet: Learned multi-view patchmatch stereo. In *Proceedings of the IEEE/CVF Conference on Computer Vision and Pattern Recognition*, pages 14194–14203, 2021. [21](#)
- [63] Jamie Watson, Michael Firman, Gabriel J Brostow, and Daniyar Turmukhambetov. Self-supervised monocular depth hints. In *Proceedings of the IEEE/CVF International Conference on Computer Vision*, pages 2162–2171, 2019. [21](#)
- [64] Alex Wong, Safa Cicek, and Stefano Soatto. Targeted adversarial perturbations for monocular depth prediction. *Advances in Neural Information Processing Systems*, 33, 2020. [3](#), [13](#)
- [65] Alex Wong, Safa Cicek, and Stefano Soatto. Learning topology from synthetic data for unsupervised depth completion. *IEEE Robotics and Automation Letters*, 6(2):1495–1502, 2021. [21](#)
- [66] Alex Wong, Xiaohan Fei, Byung-Woo Hong, and Stefano Soatto. An adaptive framework for learning unsupervised depth completion. *IEEE Robotics and Automation Letters*, 6(2):3120–3127, 2021. [21](#)
- [67] Alex Wong, Xiaohan Fei, Stephanie Tsuei, and Stefano Soatto. Unsupervised depth completion from visual inertial odometry. *IEEE Robotics and Automation Letters*, 2020. [21](#)
- [68] Alex Wong, Mukund Mundhra, and Stefano Soatto. Stereopagnosia: Fooling stereo networks with adversarial perturbations. In *Proceedings of the AAAI Conference on Artificial Intelligence*, 2021. [1](#), [3](#), [4](#), [7](#), [13](#)
- [69] Alex Wong and Stefano Soatto. Bilateral cyclic constraint and adaptive regularization for unsupervised monocular depth prediction. In *Proceedings of the IEEE/CVF Conference on Computer Vision and Pattern Recognition*, pages 5644–5653, 2019. [21](#)
- [70] Alex Wong and Stefano Soatto. Unsupervised depth completion with calibrated backprojection layers. In *Proceedings of the IEEE/CVF International Conference on Computer Vision*, pages 12747–12756, 2021. [21](#)
- [71] Chang Xiao and Changxi Zheng. One man’s trash is another man’s treasure: Resisting adversarial examples by adversarial examples. In *Proceedings of the IEEE/CVF Conference on Computer Vision and Pattern Recognition*, pages 412–421, 2020. [3](#)
- [72] Chang Xiao, Peilin Zhong, and Changxi Zheng. Enhancing adversarial defense by k-winners-take-all. *arXiv preprint arXiv:1905.10510*, 2019. [3](#)
- [73] Cihang Xie, Mingxing Tan, Boqing Gong, Jiang Wang, Alan L Yuille, and Quoc V Le. Adversarial examples improve image recognition. In *Proceedings of the IEEE/CVF Conference on Computer Vision and Pattern Recognition*, pages 819–828, 2020. [3](#)
- [74] Cihang Xie, Jianyu Wang, Zhishuai Zhang, Zhou Ren, and Alan Yuille. Mitigating adversarial effects through randomization. *arXiv preprint arXiv:1711.01991*, 2017. [3](#)
- [75] Cihang Xie, Jianyu Wang, Zhishuai Zhang, Yuyin Zhou, Lingxi Xie, and Alan Yuille. Adversarial examples for semantic segmentation and object detection. In *Proceedings of the IEEE International Conference on Computer Vision*, pages 1369–1378, 2017. [3](#), [13](#)
- [76] Cihang Xie, Zhishuai Zhang, Yuyin Zhou, Song Bai, Jianyu Wang, Zhou Ren, and Alan L Yuille. Improving transferability of adversarial examples with input diversity. In *Proceedings of the IEEE Conference on Computer Vision and Pattern Recognition*, pages 2730–2739, 2019. [2](#)
- [77] Hao-fei Xu and Juyong Zhang. Aa-net: Adaptive aggregation network for efficient stereo matching. In *Proceedings of the IEEE/CVF Conference on Computer Vision and Pattern Recognition*, pages 1959–1968, 2020. [3](#), [4](#), [13](#), [20](#), [21](#)
- [78] Yanchao Yang and Stefano Soatto. Conditional prior networks for optical flow. In *Proceedings of the European Conference on Computer Vision (ECCV)*, pages 271–287, 2018. [21](#)
- [79] Yanchao Yang, Alex Wong, and Stefano Soatto. Dense depth posterior (ddp) from single image and sparse range. In *Proceedings of the IEEE/CVF Conference on Computer Vision and Pattern Recognition*, pages 3353–3362, 2019. [21](#)
- [80] Yao Yao, Zixin Luo, Shiwei Li, Tian Fang, and Long Quan. Mvsnet: Depth inference for unstructured multi-view stereo. In *Proceedings of the European Conference on Computer Vision (ECCV)*, pages 767–783, 2018. [21](#)
- [81] Yao Yao, Zixin Luo, Shiwei Li, Tianwei Shen, Tian Fang, and Long Quan. Recurrent mvsnet for high-resolution

- multi-view stereo depth inference. In *Proceedings of the IEEE/CVF Conference on Computer Vision and Pattern Recognition*, pages 5525–5534, 2019. 21
- [82] Sergey Zagoruyko and Nikos Komodakis. Learning to compare image patches via convolutional neural networks. In *Proceedings of the IEEE conference on computer vision and pattern recognition*, pages 4353–4361, 2015. 3
- [83] Jure Žbontar and Yann LeCun. Stereo matching by training a convolutional neural network to compare image patches. *The journal of machine learning research*, 17(1):2287–2318, 2016. 3
- [84] Feihu Zhang, Victor Prisacariu, Ruigang Yang, and Philip HS Torr. Ga-net: Guided aggregation net for end-to-end stereo matching. In *Proceedings of the IEEE/CVF Conference on Computer Vision and Pattern Recognition*, pages 185–194, 2019. 3
- [85] Xizhou Zhu, Han Hu, Stephen Lin, and Jifeng Dai. Deformable convnets v2: More deformable, better results. In *Proceedings of the IEEE/CVF Conference on Computer Vision and Pattern Recognition*, pages 9308–9316, 2019. 3, 20
- [86] Yufan Zhu, Weisheng Dong, Leida Li, Jinjian Wu, Xin Li, and Guangming Shi. Robust depth completion with uncertainty-driven loss functions. *arXiv preprint arXiv:2112.07895*, 2021. 21
- [87] Yi Zhu, Karan Sapra, Fitsum A Reda, Kevin J Shih, Shawn Newsam, Andrew Tao, and Bryan Catanzaro. Improving semantic segmentation via video propagation and label relaxation. In *Proceedings of the IEEE/CVF Conference on Computer Vision and Pattern Recognition*, pages 8856–8865, 2019. 5, 14, 18
- [88] Alon Zolfi, Moshe Kravchik, Yuval Elovici, and Asaf Shabtai. The translucent patch: A physical and universal attack on object detectors. In *Proceedings of the IEEE/CVF Conference on Computer Vision and Pattern Recognition*, pages 15232–15241, 2021. 3

Supplementary Materials

A. Summary of Contents

We begin with a discussion on the existence of adversarial and universal perturbations for calibrated stereo in Sec. B. In Sec. C, we illustrate our training pipeline in Fig. 11. In Sec. D we discuss implementation details, hyperparameters, time and space requirements for training perturbations, fine-tuning with adversarial data augmentation, and retraining variants of AANet, DeepPruner, and PSM-Net. We also describe the error metrics used throughout the paper. In Sec. E, we include results for KITTI 2012 (omitted in the main text) on the performance on each stereo network against our stereoscopic universal perturbations (SUPs). We also present additional analyses on the effect of SUPs on scene geometry, on robustness of semantic classes, and on correlation between clean and perturbed features extracted for a given image and registered points between two images. In Sec. F we provide a discussion on the formulation of deformable convolutions and their use in stereo matching network. In Sec. G, we discuss the sensitivity of the proposed SUPs to number of training samples, and in Sec. H, the limitations of the SUPs as an attack and the proposed architectural designs to increase robustness of stereo networks against them. In Sec. I, we discuss potential negative impact of our work and how we can mitigate them. Finally, in Sec. J, we conclude with qualitative comparisons between perturbations crafted for the full image and the proposed 64×64 tiles. We also include additional qualitative results on the KITTI 2012, KITTI 2015 and FlyingThings3D datasets across all norms and transferability experiments.

B. On the Existence of Adversaries for Stereo

Adversarial perturbations exist for a number of tasks from classification [16, 59], object detection [75], even single image depth prediction [64]. While it may seem that they should exist for calibrated stereo, there is a qualitative difference between stereo and other single image based tasks where adversarial perturbations have been observed – such are *purely inductive* tasks: Without training data and a strong inductive prior, a single image does not enable inference of depth or labels of objects. The likelihood is flat and adversarial perturbations have free reign to modify the outcome of inference, even to control the network to yield a desired 3D scene as outcome [64]. Not so for stereo: binocular disparity is sufficient to infer depth wherever the image gradient is non-trivial, without any need for induction from a training set. One is not free to change the outcome

of inference without observable changes in the likelihood. So, the fact that adversarial perturbations exist, i.e. Stereopagnosia [68], is indeed surprising for stereo, and that they would survive architectural changes even more so.

C. Training Pipeline

In Fig. 11 we visualize the training pipeline for one iteration of our algorithm for crafting universal perturbations for stereo. Let $f_\theta(x_L, x_R) \in \mathbb{R}^{H \times W}$ be a pretrained stereo network that estimates the disparity between the left x_L and right x_R images of a stereo pair. Let $(v_L, v_R) \in \mathbb{R}^{h \times w}$ be a left and right perturbation subject to $h \mid H$ and $w \mid W$. First, we apply (v_L, v_R) to (x_L, x_R) over the entire image space, by evenly repeating the perturbation v_I across x_I with no overlap for $I \in \{L, R\}$. We then compute the gradient of the stereo network’s loss $\ell(f_\theta(\cdot), y_{gt})$ with respect to each image x_I in the stereo pair:

$$g_I^{(n)} = \nabla_{x_I^{(n)}} \ell(f_\theta(\hat{x}_L^{(n)}, \hat{x}_R^{(n)}), y^{(n)}). \quad (5)$$

For a given stereo pair (x_L, x_R) , we take the mean over the gradient with respect to the image g_I for all tiles:

$$\bar{g}_I^{(n)} = \frac{h \cdot w}{H \cdot W} \sum_{i,j} g_I^{(n)}(i, j). \quad (6)$$

This aggregated result can then be used to update the tile perturbation v_I for $I \in \{L, R\}$.

D. Implementation Details

Datasets. We optimize our perturbations on the KITTI dataset [14], which contains $\approx 47K$ 376×1240 resolution stereo pairs of real-world outdoor driving scenarios. We evaluate them on the KITTI 2012, KITTI 2015 [32], and Scene Flow [31] stereo datasets using AANet [77], DeepPruner [12], and PSMNet [5]. Due to computational limitations, we resize all images to 256×640 and adjusted disparity maps accordingly. Hence, the baseline error is slightly higher than those reported by each method.

KITTI 2012 contains 194 stereo pairs with sparse ground-truth disparities. KITTI 2015 contains 200 stereo pairs with high quality ground-truth disparity maps. Images in both datasets have dimension 376×1240 . Following the KITTI validation protocol, KITTI 2012 is divided into 160 for training and 34 for validation and KITTI 2015 is divided into 160 for training and 40 for validation. We do not use any samples from KITTI 2012 or KITTI 2015 to optimize our perturbations, and only evaluate on the validation sets.

We demonstrate that our perturbations can generalize across datasets by testing them on Scene Flow [31] – a synthetic dataset comprised of 35K training and 4370 testing 540×960 resolution images paired with ground-truth disparity maps. Like KITTI 2012 and 2015, we do not optimize our perturbations on Scene Flow and simply leverage their testing set, FlyingThings3D, in our evaluation.

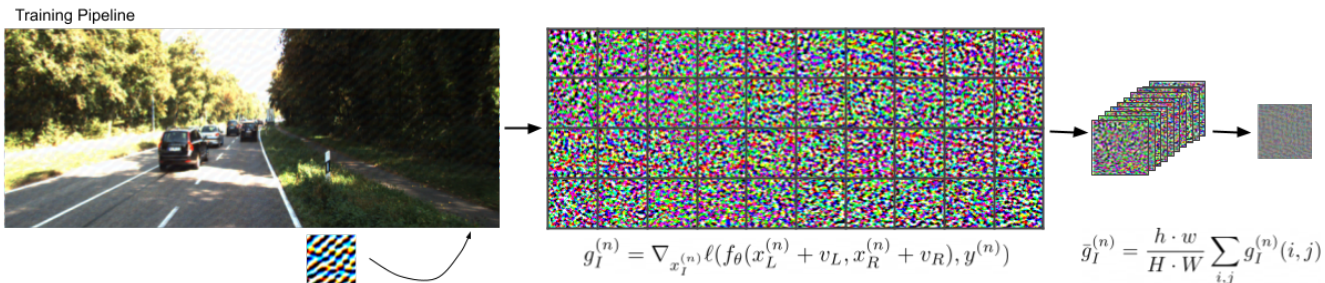


Figure 11. *Training pipeline.* Perturbations are tiled across their respective images. We take mean over the gradient with respect to each image for all tiles, which is used to update the each of the perturbations.

We used PyTorch to implement our approach. We employed the publicly available code and pretrained models of AANet, DeepPruner, and PSMNet. We note that while AANet and PSMNet released separate pretrained models for KITTI 2012 and KITTI 2015, DeepPruner released one model trained on both datasets. All three stereo networks released pretrained models for Scene Flow. We note that the pretrained model on Scene Flow of PSMNet, provided by the authors, did not reproduce the results in their paper. We obtained D1-error $> 30\%$ and EPE $> 4\text{px}$ when running on the Scene Flow test set. This is a known issue in their code repository. Hence, we fine-tuned the pretrained PSMNet model on Scene Flow, lowering the baseline D1-error to 5.57% and the EPE to 1.27px, and used this model for our experiments. We note that DeepPruner provided two model variants, DeepPruner-Best and DeepPruner-Fast. Additionally, AANet provided AANet and AANet+. We used AANet and DeepPruner-Best for all of our experiments. To analyze the robustness of semantic classes, we used the implementation and pretrained model of SDCNet [87], a segmentation network for driving scenes.

Hyper-parameters. We considered the upper norms of $\epsilon \in \{0.002, 0.005, 0.01, 0.02\}$. We searched over learning rates of $\alpha \in \{0.00005, 0.0001, 0.0002, 0.0004, 0.0008\}$. We optimized SUPs on each network using square tiles of 16, 32, 64, and 128, and the full image size 256×640 . As searching the full space of tile sizes would be intractable, we chose these as representative tiles at different scales. We omitted results for the 128×128 perturbation from the main paper due to space constraints, but describe them in Sec. E.

Training perturbations. We used an Nvidia GTX 1080Ti on a standard workstation for all of our experiments. To optimize SUPs, we iterated through the KITTI training set one time. Doing so took $\approx 5.5\text{hr}$ to craft SUPs for AANet, $\approx 7.0\text{hr}$ for DeepPruner, and $\approx 12.0\text{hr}$ for PSMNet. Our procedure took $\approx 4.3\text{GB}$ of GPU memory for AANet, $\approx 4.8\text{GB}$ for DeepPruner, and $\approx 8.8\text{GB}$ for PSMNet. As the SUPs are additive, they can be applied to an image in real time. We note that Alg. 1 uses zero initial-

ization for the perturbations. When using the estimated disparity from the clean images as pseudo ground truth, this would yield no training signal. Thus, we added zero mean Gaussian noise to the pseudo ground truth.

Fine-tuning stereo models with adversarial data augmentation. To fine-tune the stereo models with adversarial data augmentation, we used 4 Nvidia GTX 1080Ti. The models were fine-tuned for 1000 epochs on KITTI 2015 with a batch size of 8. SUPs with upper norm $\epsilon \in \{0.002, 0.005, 0.01, 0.02\}$ were selected at random and added to the training images with 50% probability. The learning rate was initially set to 1×10^{-5} , but switched to 5×10^{-6} and 1×10^{-6} after the 250th and 500th epoch, respectively. It took $\approx 9\text{hr}$, $\approx 11\text{hr}$, and $\approx 10\text{hr}$ to fine-tune AANet, DeepPruner, and PSMNet, respectively. We note that on a standard workstation, this process can take up to a week to complete.

Training stereo models with deformable convolutions. We trained a version of (i) PSMNet and (ii) DeepPruner from scratch, each with 25 deformable convolutions in the encoder. We also trained a version of (iii) PSMNet with 6 deformable convolutions, and a version of (iv) AANet without deformable convolutions. Four Nvidia GTX 1080Ti GPUs were used to train each variant, which took ≈ 4 days per model.

Both PSMNet models were trained with a batch size of 12, while DeepPruner was trained with a batch size of 16. PSMNet was trained on Scene Flow for 20 epochs, then fine-tuned on KITTI 2015 for 500 epochs. DeepPruner was first trained on Scene Flow for 64 epochs, then fine-tuned on a mixture of KITTI 2012 and KITTI 2015 for 1040 epochs. AANet was first trained on Scene Flow with a batch size of 22 for 64 epochs, fine-tuned on a mixture of KITTI 2012 and KITTI 2015 with a batch size of 12 for 1000 epochs, then fine-tuned on KITTI 2015 with a batch size of 8 for 1000 epochs. Note that DeepPruner is equivalent to PSMNet with an explicit matching module, so we sometimes refer to “DeepPruner” as “PSMNet with explicit matching” in our experiments.

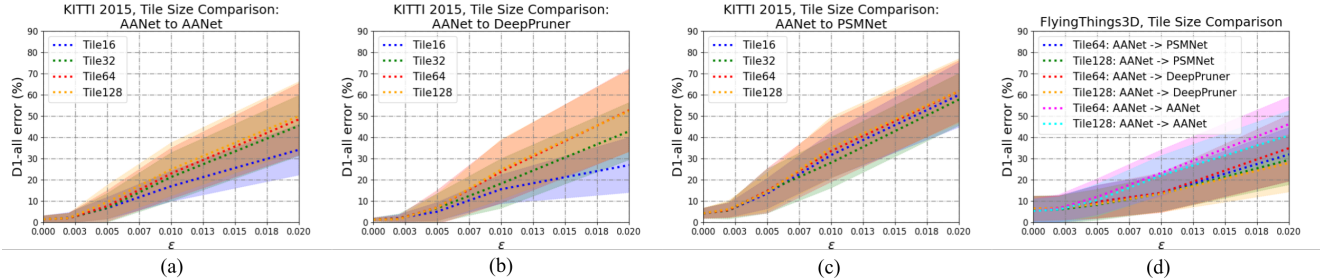


Figure 12. *Comparing tile sizes.* We optimized square tile perturbations with size 16, 32, 64, 128 on KITTI for AANet. (a, b, c) the smaller 16×16 and 32×32 tiles perform worst. (a) When applied to inputs from the dataset they are optimized on, the largest tile size 128×128 marginally outperforms 64×64 . However, (d) shows that 64×64 consistently generalizes the best from KITTI to FlyingThings3D for all three architectures. There exists a trade-off between performance on the dataset on which a set of perturbations are optimized and their ability to transfer across models and datasets, where a smaller tile size e.g. 64×64 can generalize better, but a larger tile size e.g. 128×128 may deal more damage to the network and dataset for which the perturbations are optimized.

Evaluation metrics. To evaluate the robustness of each stereo network, we use the official KITTI D1-error (the average number of erroneous pixels in terms of disparity) for KITTI 2012 and KITTI 2015 experiments:

$$\delta(i, j) = |f_{\theta}(\cdot)(i, j) - y_{gt}(i, j)|, \quad (7)$$

$$d(i, j) = \begin{cases} 1 & \text{if } \delta(i, j) > 3, \frac{\delta(i, j)}{y_{gt}(i, j)} > 5\%, \\ 0 & \text{otherwise} \end{cases} \quad (8)$$

$$\text{D1-error} = \frac{1}{\|\Omega_{gt}\|} \sum_{i, j \in \Omega_{gt}} d(i, j), \quad (9)$$

and the official Scene Flow end-point-error (EPE) metrics on FlyingThings3D for generalization experiments:

$$\text{EPE} = \frac{1}{\|\Omega_{gt}\|} \sum_{i, j \in \Omega_{gt}} \delta(i, j), \quad (10)$$

where Ω_{gt} is a subset of the image space Ω with valid ground-truth disparity annotations, $y_{gt} > 0$.

E. Experiments and Results

In the main paper, we justified our use of a 64×64 sized perturbation for our experiments. Here we expand on our search of tile sizes. We omitted results on KITTI 2012 in the main paper due to space constraints, but present them in this section. Similarly, in the main paper, we only showed results on AANet for our experiments on the effect of SUPs on scene geometry, robustness of semantic classes, and effect on the feature extractor. Here, we also present results for SUPs trained for DeepPruner and PSMNet.

Comparing tile sizes. We optimized SUPs on KITTI for AANet at each tile size and attacked AANet (Fig. 12-(a)), DeepPruner (Fig. 12-(b)), and PSMNet (Fig. 12-(c)). The 16×16 and 32×32 tiles consistently performed worst, which justifies our choice not to explore smaller tiles. The 128×128 tile performed negligibly better than the 64×64

tile. However, Fig. 12-(d) shows that the 64×64 tile generalizes better than the 128×128 perturbation across all networks on FlyingThings3D. For SUPs with $\epsilon = 0.02$, 64×64 achieves 46.14% error on AANet, 34.87% on DeepPruner and 31.93% on PSMNet, while 128×128 achieves 40.84%, 27.89%, and 29.33% respectively. As demonstrated in the main paper, the full-size perturbations do worse than both, at 36.09% error on AANet, 23.28% on DeepPruner, and 25.35% on PSMNet. We note that, in choosing the tile size, there is a clear trade-off between the performance on the model and dataset for which SUPs are optimized and the generalization to novel architectures and data distributions. For the purpose of universal perturbations that transfer across architectures and datasets, we choose the 64×64 tile size. However, given our results, we leave it up to the user to decide which tile size best suits their use case.

Generalization across architectures and data. We optimized three sets of 64×64 SUPs on KITTI for AANet, DeepPruner, and PSMNet, respectively. In Fig. 13, we attack each network with each set of SUPs on three datasets: KITTI 2012 and 2015 (real datasets of outdoor driving scenarios), and Flyingthings3D (synthetic dataset of random “flying” objects). We report D1-error for KITTI 2012, and 2015, and EPE for FlyingThings3D. In the main paper, we omitted results for KITTI 2012 due to space constraints, but present them here.

In Fig. 13-(a), we add the perturbations optimized for each network to the input stereo pairs from KITTI 2015 for all three networks. Here, KITTI 2015 is a held out data split from KITTI so the distribution of scenes follow that of the training set. When a set of perturbations are applied to the network for which they are optimized, as expected, they tend to be the most successful at corrupting the outputs of the network. We note that AANet (red lines) is consistently more robust against attacks and PSMNet (blue lines) is consistently more susceptible.

In Fig. 13-(b), we add the perturbations optimized for

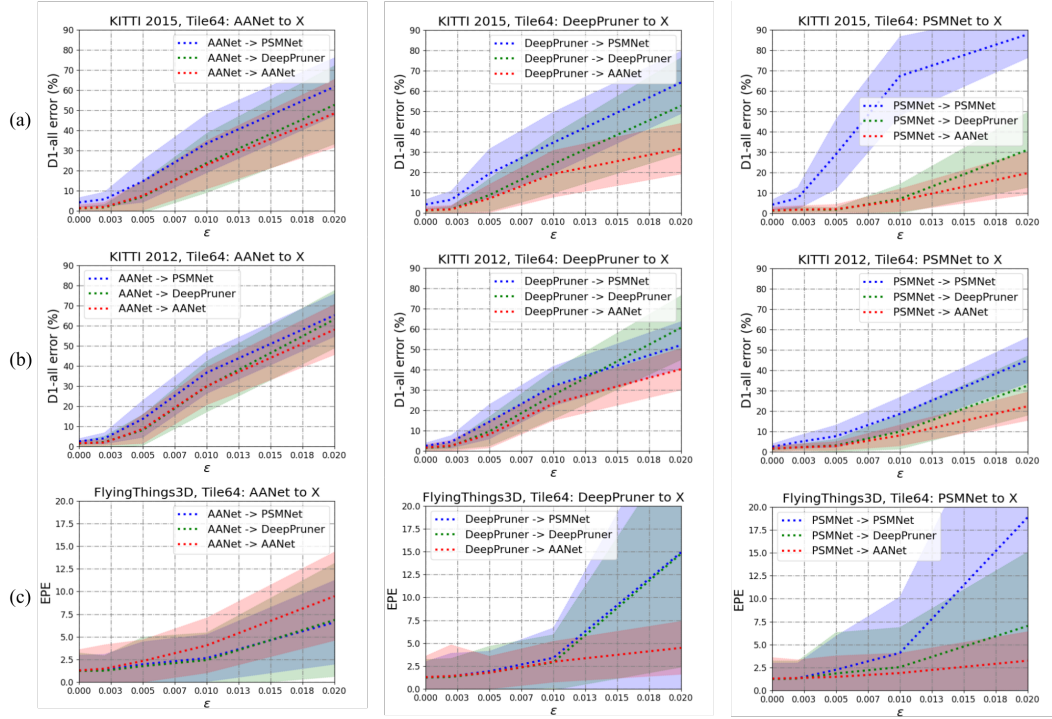


Figure 13. *Generalization across architectures and datasets.* We optimized stereoscopic universal perturbations on AANet, DeepPruner and PSMNet for KITTI (real dataset of outdoor driving scenario) and tested them on three datasets. We measure D1-error for KITTI 2012 and 2015, and EPE for FlyingThings3D. For all three networks, we add the perturbations optimized for each network to input stereo pairs from (a) KITTI 2015, (b) KITTI 2012, and (c) FlyingThings3D. The proposed universal perturbations optimized for a single network on KITTI can fool different network architectures across multiple datasets.

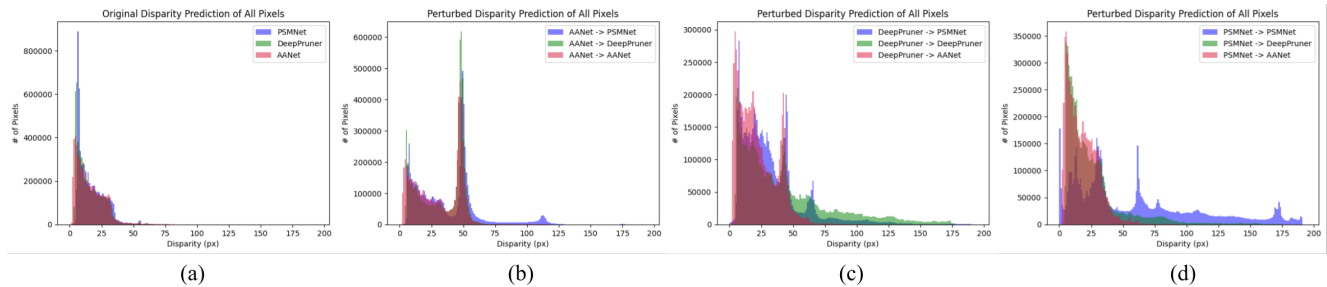


Figure 14. *Distribution of disparities before and after adding perturbations.* (a) Distribution of estimated disparities for AANet, DeepPruner and PSMNet on clean (no added perturbations) stereo pairs. Most disparities are concentrated at 2 pixels. Adding perturbations optimized for (b) AANet, (c) DeepPruner, and (d) PSMNet on KITTI to all three models. Disparities shift from 2 pixels to ≈ 50 pixels in (b), and to ≈ 40 and ≈ 60 pixels in (c) and (d). We note that in all cases, the disparities grow larger, meaning that the estimated depth grows smaller, so the perceived distances to objects populating the scene are closer than they should be.

each network to input stereo pairs from KITTI 2012 for all three networks. Like KITTI 2015, KITTI 2012 is also a held out data split from KITTI, but contains different objects populating the scene. We observe similar trends as KITTI 2015, where AANet is still the most robust and PSMNet the least robust. We note that for all KITTI 2012 and 2015 experiments, all stereo models are trained on KITTI.

In Fig. 13-(c), we test the generalization of our perturbations across different data distributions. To this end, we add the perturbations optimized for each network to input

stereo pairs from FlyingThings3D for all three networks. Here, FlyingThings3D is a synthetic dataset comprised of random “flying” objects where the scene distribution is differs greatly from that of KITTI. For this experiment, all of the stereo models are trained on Scene Flow datasets, which consists of Monkaa, Driving, and FlyingThings3D. Despite being optimized for a single network on KITTI, each pair of perturbations are able fool different network architectures trained on different datasets comprised of different scene distributions in a different domain. To the best of our knowl-

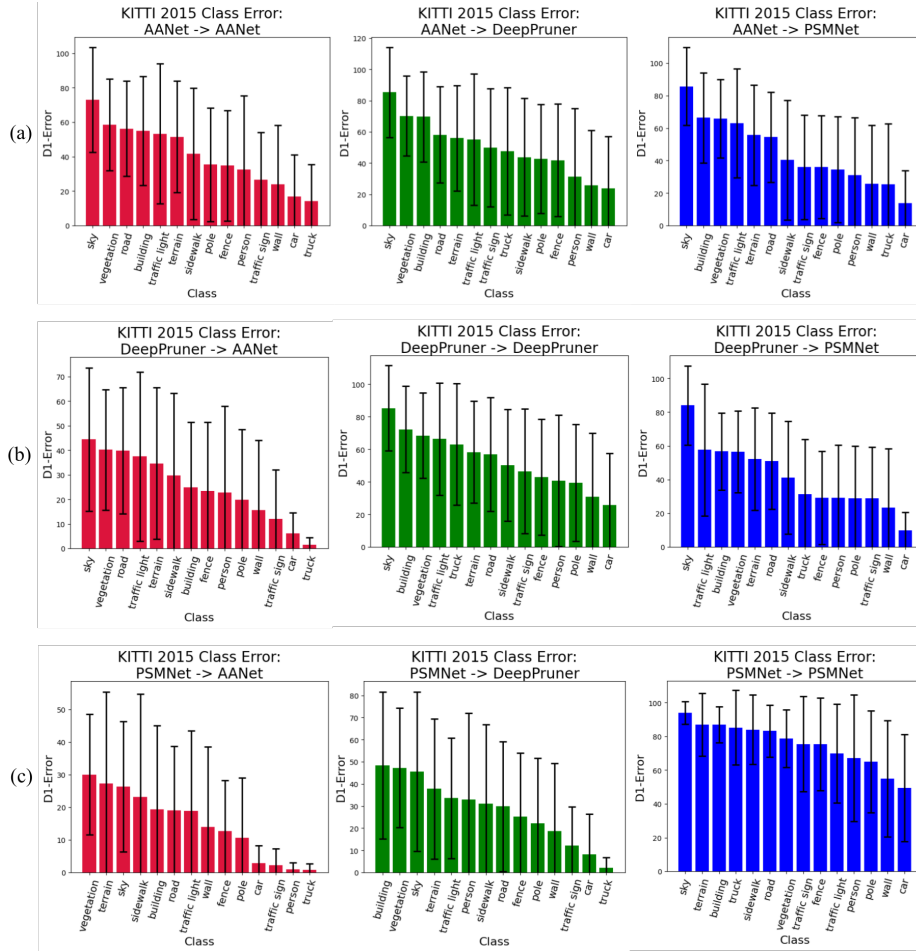


Figure 15. *Quantitative evaluation on KITTI 2015, D1-error for each semantic class.* We use SDCNet, an off-the-shelf semantic segmentation network to partition the image domain of stereo pairs from KITTI 2015 into semantic classes. We show the effect of perturbations optimized on KITTI on different classes for (a) AANet, (b) DeepPruner, and (c) PSMNet. Each semantic class exhibits a different level of robustness against adversaries. However, there are some common trends. For all perturbations and across all networks, the classes that are most susceptible are “building”, “vegetation”, “sky” and “road”. The least susceptible are “car”, “person”, “pole” and “traffic sign”.

edge, we are the first to demonstrate stereoscopic universal perturbations that generalize across architectures and data.

Effect on scene geometry. In the main text, we showed that the mode of the distribution of disparities shifts from ≈ 2 pixels to ≈ 50 pixels when each network is attacked by SUPs optimized for AANet. To more effectively quantify how SUPs affect the predicted scene geometry, we plotted the distributions of disparity estimates for all networks tested, where clean (no added perturbation) baseline disparities are shown in Fig. 14-(a) and disparities for perturbed stereo pairs are shown in Fig. 14-(b,c,d). Specifically, we consider the change in disparity distribution for SUPs optimized and tested on the same network and SUPs optimized on other networks. In Fig. 14-(b), we apply perturbations optimized for AANet, in Fig. 14-(c) DeepPruner, and in Fig. 14-(d) PSMNet. We note that all of these experiments were performed on the KITTI 2015 validation set.

As mentioned in the main text, there is a systemic increase in the estimated disparities when perturbations are added to the input stereo pairs; in other words, a decrease in depth, where objects are perceived as closer than they really are. While the general trend is present for all networks, the effect is varied as SUPs optimized for AANet causes a sharp mode at ≈ 50 pixels whereas SUPs optimized for PSMNet and DeepPruner also create modes at ≈ 40 pixels and ≈ 60 pixels. While we do not conduct additional experiments to determine the reason for this bias, we hypothesize that it is induced by the dataset that the perturbations are trained on and will leave this analysis to future works. Interestingly, the same effect transfers to other datasets as well e.g. KITTI 2012 and FlyingThings3D, where visualizations of the output disparities are consistently closer than those estimated from clean images. Indeed, this shows that there are common vulnerabilities across images not only within

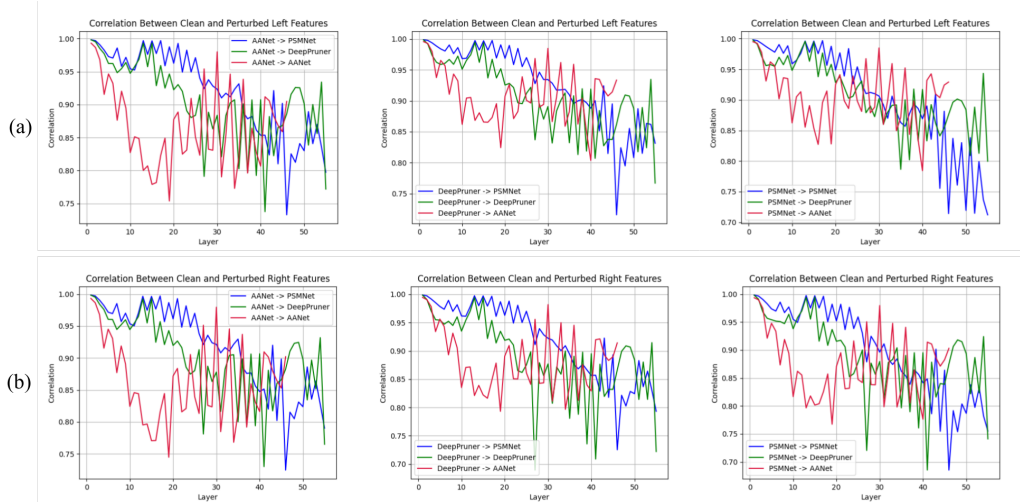


Figure 16. *Effect on clean and perturbed left and right feature maps.* Perturbations optimized for AANet, DeepPruner and PSMNet were added to KITTI 2015 stereo pairs. Correlation was computed between the (a) clean and perturbed left stereo images, and (b) clean and perturbed right stereo images. In both cases, the correlation decreased between the clean and perturbed feature maps. The perturbation signal is amplified by the encoding function as it is fed through the layers in a forward pass.

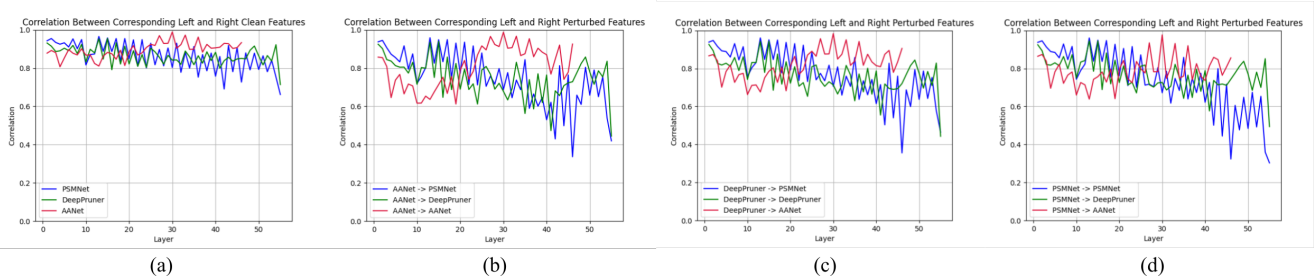


Figure 17. *Effect on corresponding left and right feature maps.* Perturbations optimized for AANet, DeepPruner and PSMNet were added to each stereo pair in KITTI 2015. (a) Correlation was computed between corresponding left and right clean features. Correlation was then computed between corresponding left and right perturbed features, using a perturbation optimized for AANet (b), DeepPruner (c), and PSMNet (d). The perturbed features become uncorrelated relative to the clean features. This suggests that universal perturbations cause similar regions in the RGB domain to be dissimilar in the embedding space, resulting in incorrect correspondences.

a dataset, but across datasets and domains. We illustrate this phenomenon in Fig. 1, Fig. 3 and Fig. 8 in the main text, where larger disparities or smaller depths are depicted as brighter (yellow) regions in the colormap. We also observe a similar phenomenon in the additional qualitative results provided below (see Fig. 22, Fig. 23, Fig. 24, Fig. 28, Fig. 29, Fig. 30).

Robustness of semantic classes. In the main text, we observed that different semantic classes exhibit different levels of robustness against adversaries. We measured the per class error of the disparities estimated by AANet when attacked by a perturbation optimized for AANet. For completeness, we show the per class errors for each network when attacked by adversaries optimized for AANet (Fig. 15-(a)) DeepPruner (Fig. 15-(b)) and PSMNet (Fig. 15-(c)). To this end, we use SDCNet [87], an off-the-shelf semantic segmentation network to partition the image domain of stereo pairs from KITTI 2015 into seman-

tic classes. We observe that each semantic class exhibits a different level of robustness against adversaries. However, there are some common trends across all the networks. Fig. 15 shows that for all perturbations and across all networks, the classes that are most susceptible are “building”, “vegetation”, “sky” and “road”. The least susceptible are “car”, “person”, “pole” and “traffic sign”. We note that the most robust object classes tend to be those with rich textures. In contrast, the least robust classes are those that tend to be comprised of largely homogeneous regions e.g. “sky”, “road”. We hypothesize that this is due to the nature of the correspondence problem. Because stereo networks employ feature matching as a measure of data fidelity, regions with sufficiently exciting textures tend to have unique correspondences; whereas, there exists inherent ambiguity in locating correspondences in textureless, repeating patterns, and homogeneous regions. This leads to the network relying on the regularizer or the prior (learned from data) to fill in the

gaps. The information of the regularizer is stored in the weights or parameters of a network via the training process. As the perturbation signal corrupts the activations of feature maps on which the weights operate on, it is thus corrupting the regularizer or prior, and so the prediction for textureless and homogeneous regions is worse.

Effect on Feature Maps. In the main text, we discussed the effect of stereoscopic universal perturbations (SUPs) on the encoder, or embedding function, for AANet. Here we show results for all three networks in Fig. 16. We added the perturbations optimized for each network into stereo pairs from KITTI 2015 and forwarded them through each network. Similarly, we also fed clean stereo pairs without any added perturbations into each network. The per layer activations of the encoder, shared between the left and right images, were extracted for clean and perturbed stereo pairs. Correlation was then computed between the clean and perturbed left feature maps, and clean and perturbed right feature maps. Fig. 16-(a) shows the correlation between clean and perturbed left image feature maps for each network, while Fig. 16-(b) shows the same for the right image. In both cases, the correlation decreases between the clean and perturbed feature maps. This demonstrates that even though the input perturbation is constrained to be some ϵ small, the perturbation signal is amplified by the encoding function as it is fed through the layers in a forward pass. In effect, this can cause a network to output significantly different results.

However, stereo networks employ an explicit matching mechanism. Even though the perturbations may cause the clean and perturbed features to be different, as long as the true corresponding (registered) pixels between the left and right images are “close” in the embedding space, the correct disparity between the two images can be found. Fig. 17 shows that indeed the perturbations not only causes clean and perturbed feature maps to be different, but also the corresponding registered left and right features to be different. Specifically, Fig. 17-(a) shows that registered clean features are well-correlated throughout all of the features maps in the encoder. This is expected. However, Fig. 17-(b, c, d) shows that left and right registered perturbed features become increasingly uncorrelated relative to the clean features as they pass through the shared encoder. This suggests that our universal perturbations cause similar regions in the RGB domain to become dissimilar in the embedding space. As registered points in the images are no longer similar, this in turn fools the explicit matching modules to find incorrect correspondences, resulting in the wrong disparity estimates. We note that in both Fig. 16 and Fig. 17, the correlation of the features of AANet increase from layers 20 to 30. This phenomenon is present for all adversaries, and coincides with the use of deformable convolution in AANet. We conjecture that deformable convolutions may be related to the robustness of AANet. Hence, we use this observation to motivate

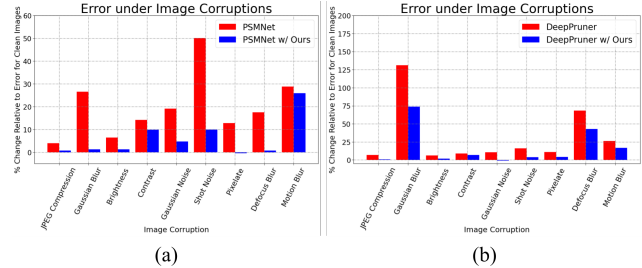


Figure 18. *Robustness to Image Perturbations.* (a) Robustness of PSMNet, PSMNet with 25 layers of deformable convolutions, (b) DeepPruner, and DeepPruner with 25 layers of deformable convolutions against different types of image corruptions.

the use of deformable convolutions (and explicit matching modules like correlation or PatchMatch) as part of our proposed architectural designs to increase robustness against SUPs (see Sec. 5 in the main paper).

Robustness to Image Perturbations. In the main text, we discussed the robustness of PSMNet and PSMNet with 25 DCs against common image corruptions i.e. lossy (JPEG) compression, Gaussian, defocus and motion blur, shot noise (Fig 10-(d)). As shown in Fig. 18-(a) and also in Fig 10-(d), our design improves over PSMNet by an average of 70% to common image perturbations. Fig. 18-(b) shows that DeepPruner (red), like PSMNet, is also susceptible to noise and blurring. In the case of Gaussian blur with a kernel size of 5 and a standard deviation of 1, the error increases by as much as 131%. Our design of DeepPruner with 25 DCs (blue) is significantly more robust across all tested common image corruptions. There is an improvement of 43% on gaussian blur and 37% on defocus blur. Moreover, our design improves by 76% on shot noise and 60% on average.

F. On Deformable Convolution

In the main paper, we found that replacing convolutional layers with deformable convolutional layers can increase the robustness of stereo networks. For the sake of completeness, in this section, we motivate the use of deformable convolutions in convolutional neural networks (CNNs) through their formulation. We then describe the use of deformable convolution in stereo matching networks.

Motivation. Due to rigid components, CNNs are limited at modeling geometric variations in object viewpoint, pose, scale, and part deformation. Conventional architectures are comprised of layers of fixed size convolutional filters over a regular grid with limited receptive field. While feature pyramids using spatial downsampling (e.g. max pooling and strided convolution) allow for modeling different scales of objects populating the scene, extensive geometric data augmentations are necessary to capture the variations listed above. Yet, it is not possible to fully capture all variations

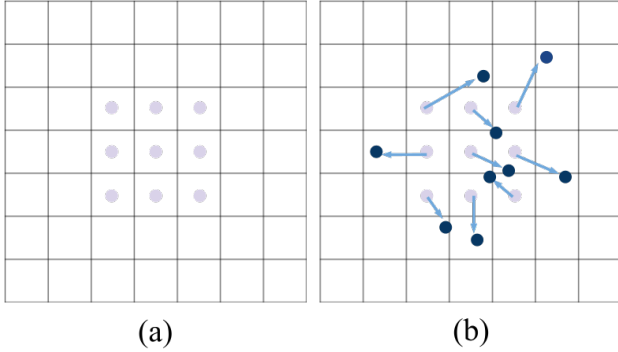


Figure 19. *Deformable convolution*. (a) The sampling grid of a standard 3×3 convolution. (b) The sampling locations of a deformable convolution (dark blue), adaptively offset from the regular sampling grid.

in the data. Additionally, the effective field of view is limited to a local neighborhood sampled regularly, which is ignorant of object boundaries. Hence, [9, 85] proposed deformable convolutions to learn object deformations by directly conditioning on the data. Deformable convolution adds 2D offsets, predicted based on the input feature map, to the sampling grid of standard convolution. It allows the sampling grid to deform freely and hence capture visibility phenomena such as occlusions, as visualized in Fig. 19.

Formulation. Let \mathbf{x} be an input feature map and \mathbf{y} be an output feature map. The standard 2D convolution is a two-step operation: 1) sample \mathbf{x} over a regular grid \mathcal{R} ; 2) compute a weighted sum of the sampled values to generate \mathbf{y} . Formally, for each location \mathbf{p}_0 in \mathbf{y} ,

$$\mathbf{y}(\mathbf{p}_0) = \sum_{\mathbf{p}_n \in \mathcal{R}} \mathbf{w}(\mathbf{p}_n) \cdot \mathbf{x}(\mathbf{p}_0 + \mathbf{p}_n) \quad (11)$$

where \mathbf{p}_n are the locations in \mathcal{R} .

In deformable convolution, the sampling grid \mathcal{R} are augmented with offsets $\{\Delta\mathbf{p}_n | n = 1, \dots, |\mathcal{R}|\}$. Eqn. 11 extends to

$$\mathbf{y}(\mathbf{p}_0) = \sum_{\mathbf{p}_n \in \mathcal{R}} \mathbf{w}(\mathbf{p}_n) \cdot \mathbf{x}(\mathbf{p}_0 + \mathbf{p}_n + \Delta\mathbf{p}_n). \quad (12)$$

Here, we sample at offset locations $\mathbf{p}_n + \Delta\mathbf{p}_n$. Because the offset \mathbf{p}_n can be fractional, $\mathbf{x}(\mathbf{p}_0 + \mathbf{p}_n + \Delta\mathbf{p}_n)$ may not correspond to an actual element and is subject to quantization effects. Hence, $\mathbf{x}(\mathbf{p}_0 + \mathbf{p}_n + \Delta\mathbf{p}_n)$ is computed via bilinear interpolation.

Use in stereo matching. AANet [77] introduce an intra-scale aggregation (ISA) module for cost aggregation, designed to adaptively sample points from regions of similar disparity. The authors intuit that adaptive sampling prevents the edge-fattening issue at disparity discontinuities [55]. Formally, let $\mathbf{C} \in \mathbb{R}^{D \times H \times W}$ be a cost volume with maximum disparity D , height H , and width W . For K^2 sampling

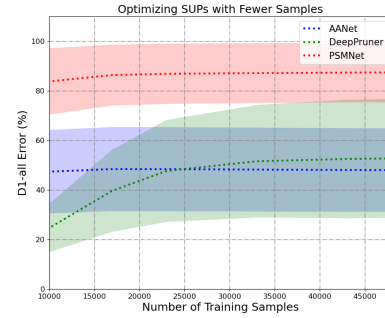


Figure 20. *Sample efficiency*. We optimize SUPs for AANet, DeepPruner and PSMNet with fewer samples and test their effectiveness on KITTI 2015. SUPs for AANet and PSMNet be still be effective even when optimized with 79% fewer samples; the effectiveness of SUPs optimized for DeepPruner start to decrease when optimized with less than 60% of the dataset.

points, the ISA computation is

$$\tilde{\mathbf{C}}(d, \mathbf{p}) = \sum_{k=1}^{K^2} w_k \cdot \mathbf{C}(d, \mathbf{p} + \mathbf{p}_k + \Delta\mathbf{p}_k) \quad (13)$$

where $\tilde{\mathbf{C}}(d, \mathbf{p})$ is the aggregated cost at pixel \mathbf{p} for disparity d , w_k is the weight for point k , \mathbf{p}_k is a fixed offset from \mathbf{p} , and $\Delta\mathbf{p}_k$ is a learned offset. Since the formulations are similar, ISA is implemented with deformable convolution. We note that in addition to the ISA module, AANet also employs deformable convolutions in its encoder to reduce sampling across object boundaries, which minimizes the bleeding effect often seen in backprojected point clouds. While the proposed use case is mainly to handle object deformation and variations in view point, we found that deformable convolutions are amicable towards defending against adversaries as their formulation naturally allows for “avoiding” certain signals e.g. occlusion boundaries, part deformation, and perhaps adversarial perturbations present in the input.

G. On Sample Efficiency

In Fig 5, 8 of main text, SUPs were optimized using KITTI (outdoor driving, real domain) and are added to images from the FlyingThings3D test set (randomly generated scenes, synthetic), part of the Scene Flow [32] datasets. These perturbed images are fed to AANet [77], DeepPruner [12] and PSMNet [5] that were trained on Scene Flow. For this particular set of experiments, our SUPs were trained with substituted data from KITTI and zero-shot transferred to FlyingThings3D.

In this section, we study the sample efficiency of SUPs. We optimized SUPs for AANet, DeepPruner and PSMNet using the KITTI raw dataset for varying training sample sizes. Fig. 20 shows that SUPs for AANet and PSMNet

are still effective when optimized with just 21% of KITTI; whereas SUPs for DeepPruner start to decrease in effectiveness when we remove 60% of the samples.

H. Limitations

While we have demonstrated stereoscopic universal perturbations (SUPs) that generalize across network architectures, datasets and domains and showed that deformable convolutions and explicit matching can help mitigate them, there exist limitations on both fronts. Despite reaching as high as 87% in D1-error on PSMNet, SUPs has a limited effectiveness on AANet and reaches 50% D1-error – this is equivalent to half of the perceived scene being corrupted. In none of our experiments do the error reach 100%, meaning that there are still portions of the scene that are reasonably correct.

We note that such perturbations are not undefendable; we showed that fine-tuning with adversarial data augmentation does mitigate them to some extent, but not fully. For example D1-error decreased from 87.72% to 2.96% for PSMNet when attacked by the adversary it was trained on, but when attacked by new adversaries, it still has a 35.75% error. While our proposed architecture designs involving deformable convolutions and explicit matching does help, they also do not fully mitigate the attack.

Our scope is limited to stereo [5, 12, 46, 77]; however, the component proposed in our architectural design. i.e. deformable convolutions and inductive biases like explicit matching, are used in many geometric problems such as optical flow [2, 25–27, 58, 60, 78], multi-view stereo [7, 17, 62, 80, 81], monocular depth prediction [13, 15, 45, 47, 52, 63, 69], and depth completion [21, 29, 43, 65–67, 70, 79, 86]. These are problems where adversarial and universal perturbations are less studied. So there is a long road ahead, but we hope that our findings will be useful towards realizing robustness deep neural networks.

I. Discussion of Potential Negative Impact

Deep learning models have been extensively deployed for many applications. Hence, adversarial perturbations have been treated as a security concern. These concerns were initially far fetched, as adversarial perturbations were optimized per-image instance; it would be computationally infeasible to corrupt a model in real-time. Yet, the discovery of universal adversarial perturbations made the security threat more realistic.

We showed that stereoscopic universal perturbations (SUPs) that generalize across architecture and data exist. These can be applied effectively to attack models in the black-box setting, and so appear to present a more immediate security threat. Yet, we believe these perturbations will not cause damage outside of the academic setting. While

our perturbations can be realized as a filter to be placed on top of a camera lens, autonomous agents typically have a myriad other sensors. An autonomous system should not fail due to a corrupted disparity map as long as it can rely on sensor measurements from other sources.

Rather, we have used stereoscopic universal perturbations to better understand the robustness of stereo networks. By identifying how SUPs can corrupt stereo networks, we were able to motivate several architectural designs (see Sec. 5, main text) that ultimately improve the robustness of stereo models. Adversarial perturbations expose inherent problems with our deep networks – yet, we view them as an opportunity to unravel our black-box models and develop more robust representations.

Nonetheless, to mitigate them, one can redesign models with the proposed architectural changes, leverage adversarial data augmentation to fine-tune existing models, or utilize techniques to denoise, purify, or rectify the input as discussed in our Related Works section (Sec. 2, main text). Additionally, we will also restrict code and perturbations usage via our release license.

J. Additional Qualitative Results

In Fig. 21 we show SUPs optimized for AANet, DeepPruner, and PSMNet on the KITTI dataset. Each panel of two rows shows SUPs optimized over the full 256×640 image and the 64×64 sized perturbations, tiled across the image domain, for each method. The tiled perturbations are then used for each subsequent visualization. We note that for all full image size SUPs, there are structural artifacts biased by the scenes in the dataset. For instance, full image size SUPs for PSMNet shows a road pattern in the both perturbation images. As a result, these dataset specific structures limit the generalization of SUPs that were optimized over the full image. Unlike them, 64×64 tiles do not contain any of these structures as they are spatially invariant, enabling them to transfer across datasets and domains.

Next, we demonstrate attacks against each model using the SUPs trained for it. We show the perturbed stereo pair, the original disparities estimated from clean stereo pairs and the corrupted disparities estimated from the perturbed stereo pair for KITTI 2015 (Fig. 22), KITTI 2012 (Fig. 23), and FlyingThings3D (Fig. 24). To demonstrate how an attack varies for different upper norms, we attack each network for scenes from KITTI 2015 using perturbations with upper norm $\epsilon \in \{0.002, 0.005, 0.01, 0.02\}$; we look at AANet in Fig. 25, DeepPruner in Fig. 26, and PSMNet in Fig. 27. As expected, as the upper norm ϵ increases, we also observe more corruption in the disparity map. The corrupted regions are generally estimated as “closer” to the camera. We conclude by visualizing transferability of the SUPs to PSMNet across different datasets in Fig. 28, Fig. 29, and Fig. 30.

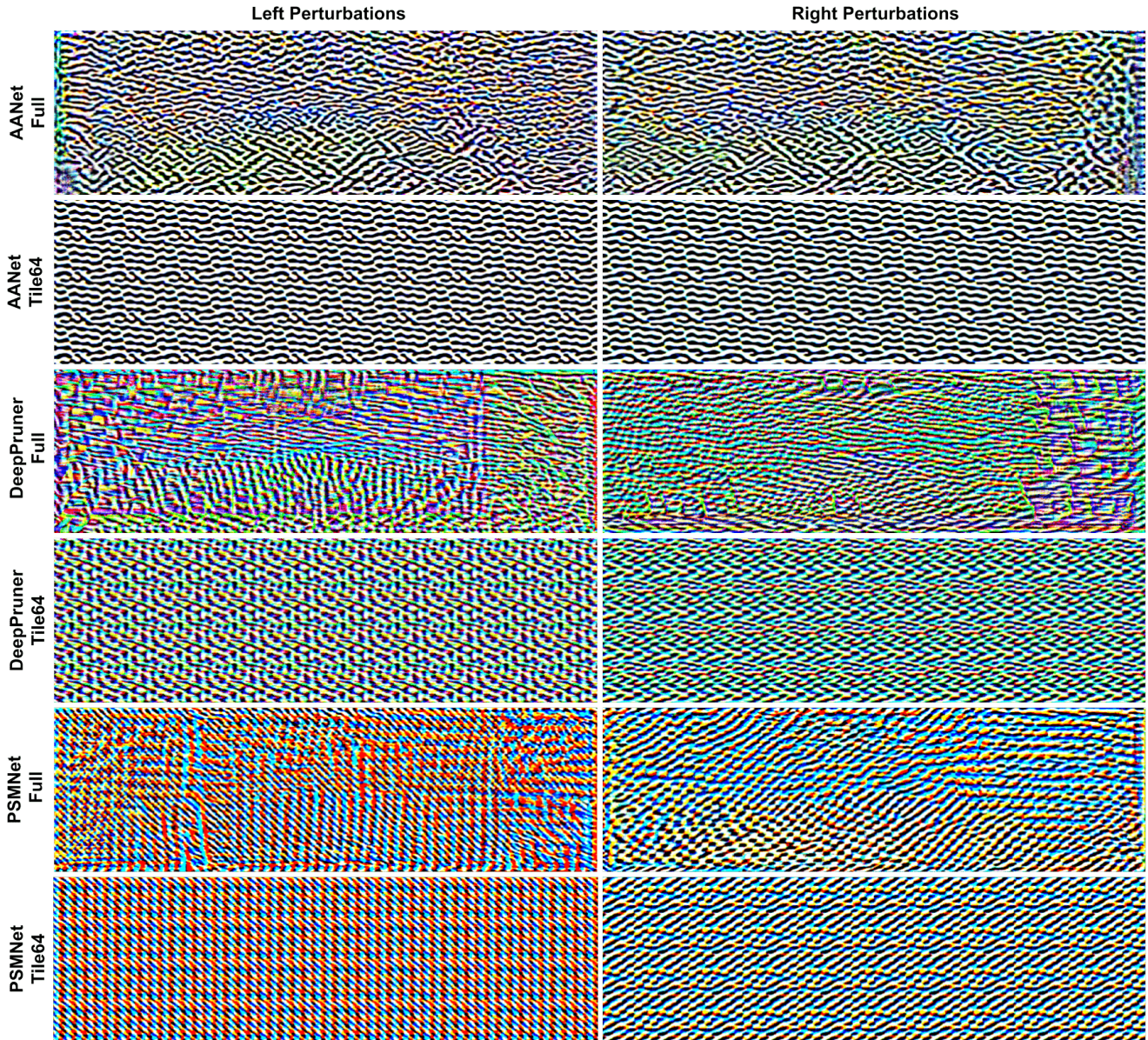


Figure 21. *Examples of Stereoscopic universal perturbations (SUPs) optimized for AANet, DeepPruner, and PSMNet on the KITTI dataset. Each panel of two rows shows SUPs optimized over the full 256×640 image and the 64×64 sized perturbations, tiled across the image domain, for each method. We note that for all full image size SUPs, there are structural artifacts biased by the scenes in the dataset, which limits their generalization capabilities.*

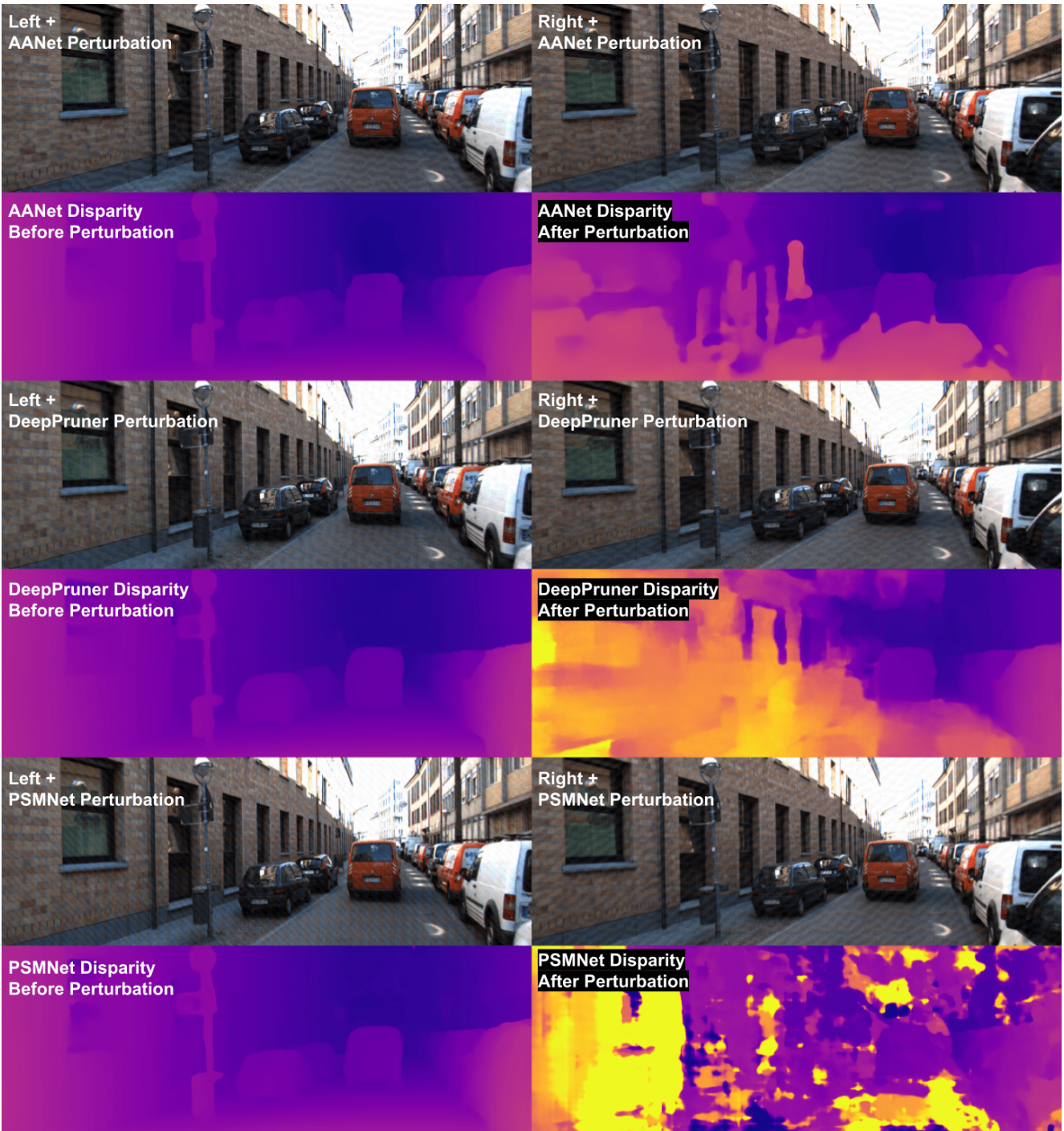


Figure 22. Attacking AANet, DeepPruner, and PSMNet on a scene from KITTI 2015 using the SUP trained for each model.



Figure 23. Attacking AANet, DeepPruner, and PSMNet on a scene from KITTI 2012 using the SUP trained for each model.

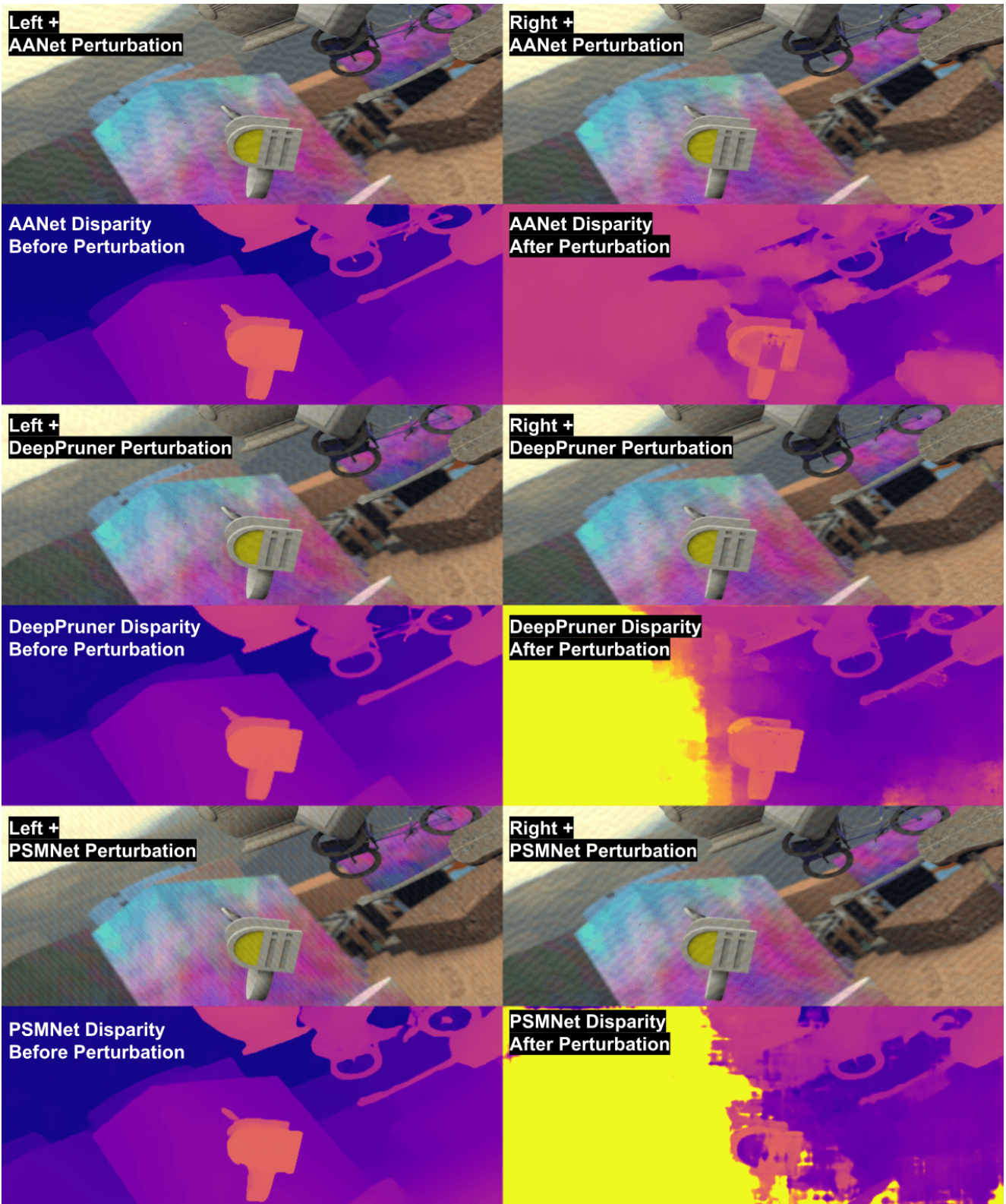


Figure 24. Attacking AANet, DeepPruner, and PSMNet on a scene from FlyingThings3D using the SUP trained for each model.

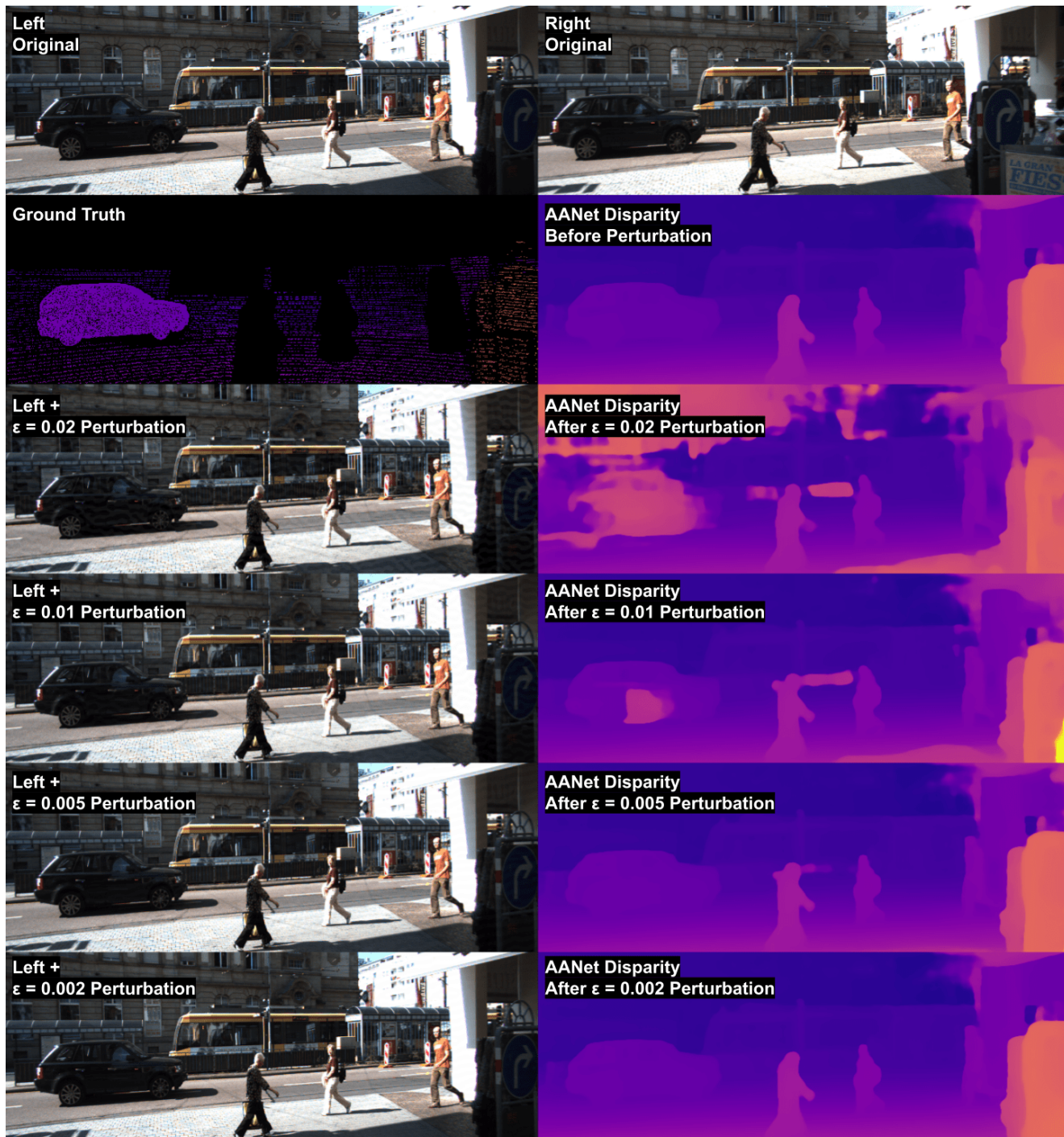


Figure 25. Attacking AANet at different upper norms $\epsilon \in \{0.002, 0.005, 0.01, 0.02\}$ for a scene from KITTI 2015.

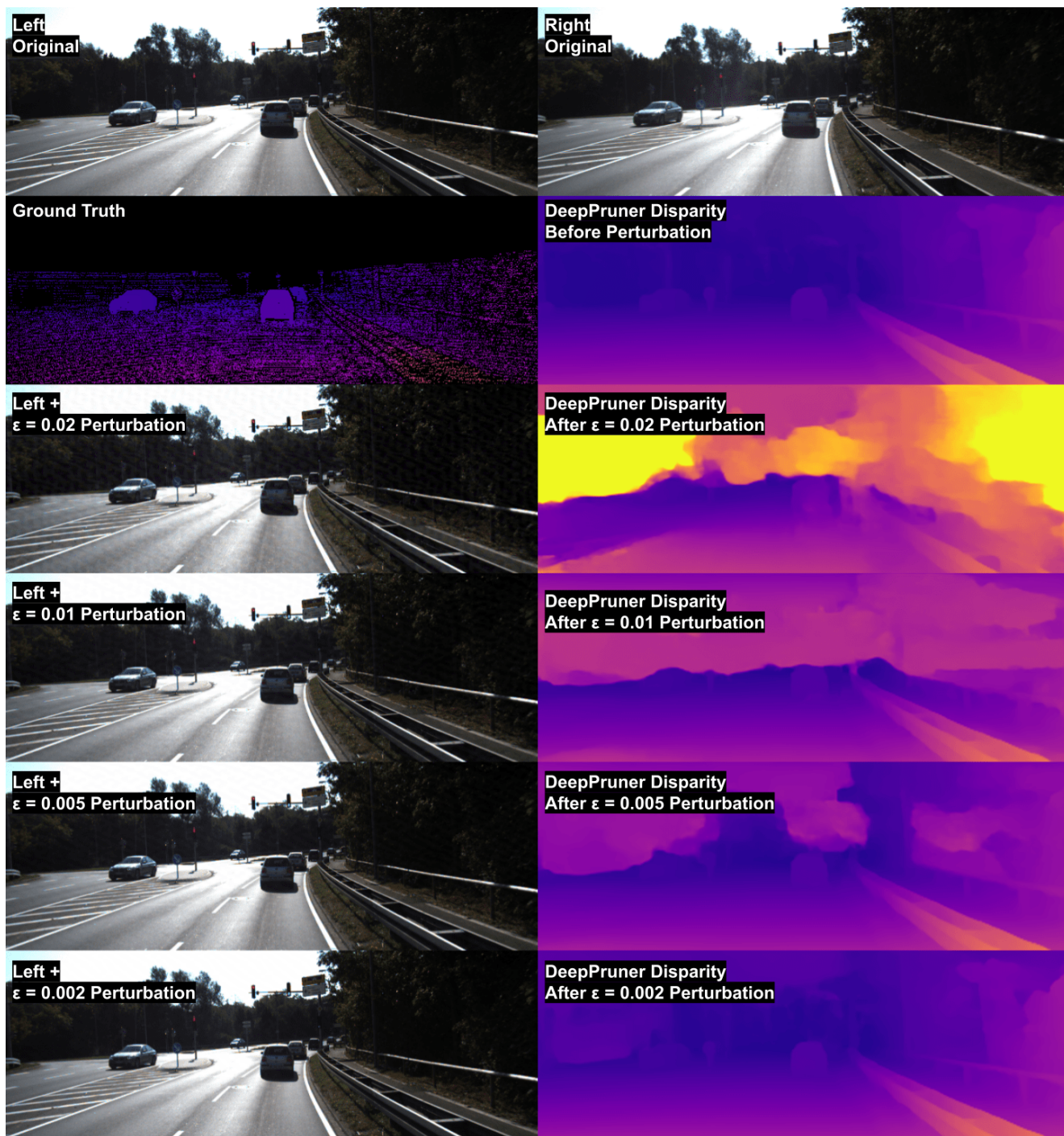


Figure 26. Attacking DeepPruner at different upper norms $\epsilon \in \{0.002, 0.005, 0.01, 0.02\}$ for a scene from KITTI 2015.

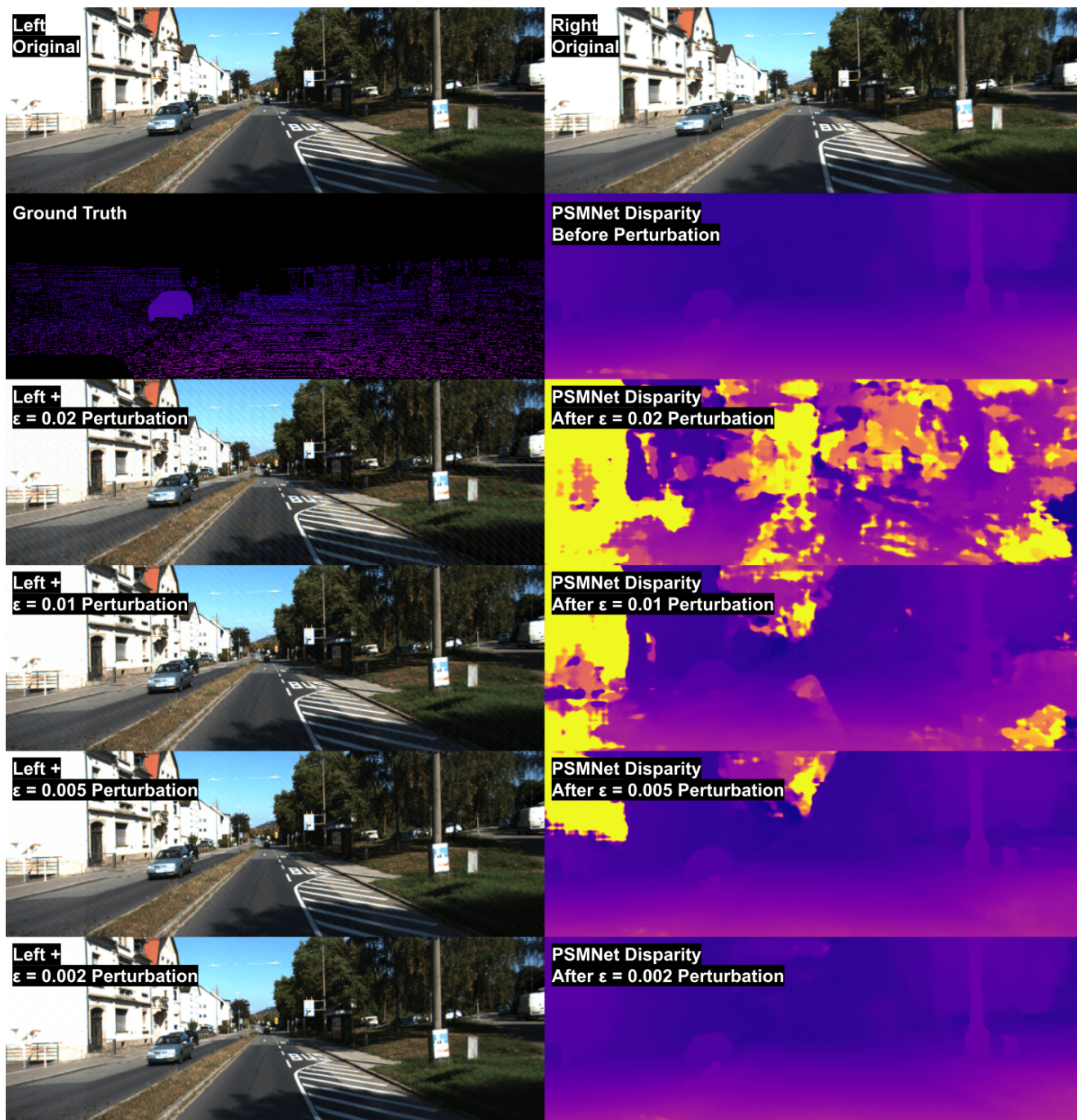


Figure 27. Attacking PSMNet at different upper norms $\epsilon \in \{0.002, 0.005, 0.01, 0.02\}$ for a scene from KITTI 2015.

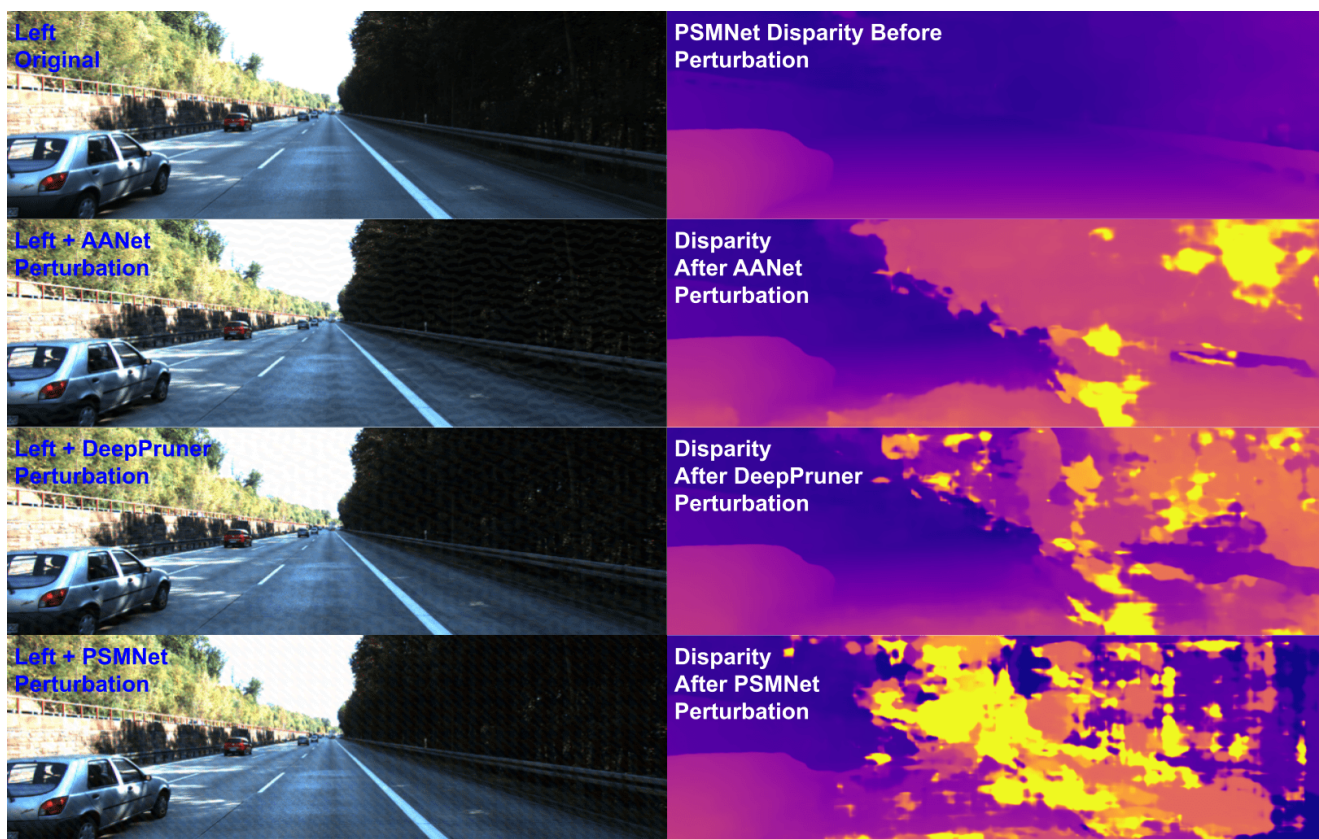


Figure 28. Attacking PSMNet for a scene from KITTI 2015 with a stereoscopic universal perturbations optimized on KITTI for AANet, DeepPruner, and PSMNet.

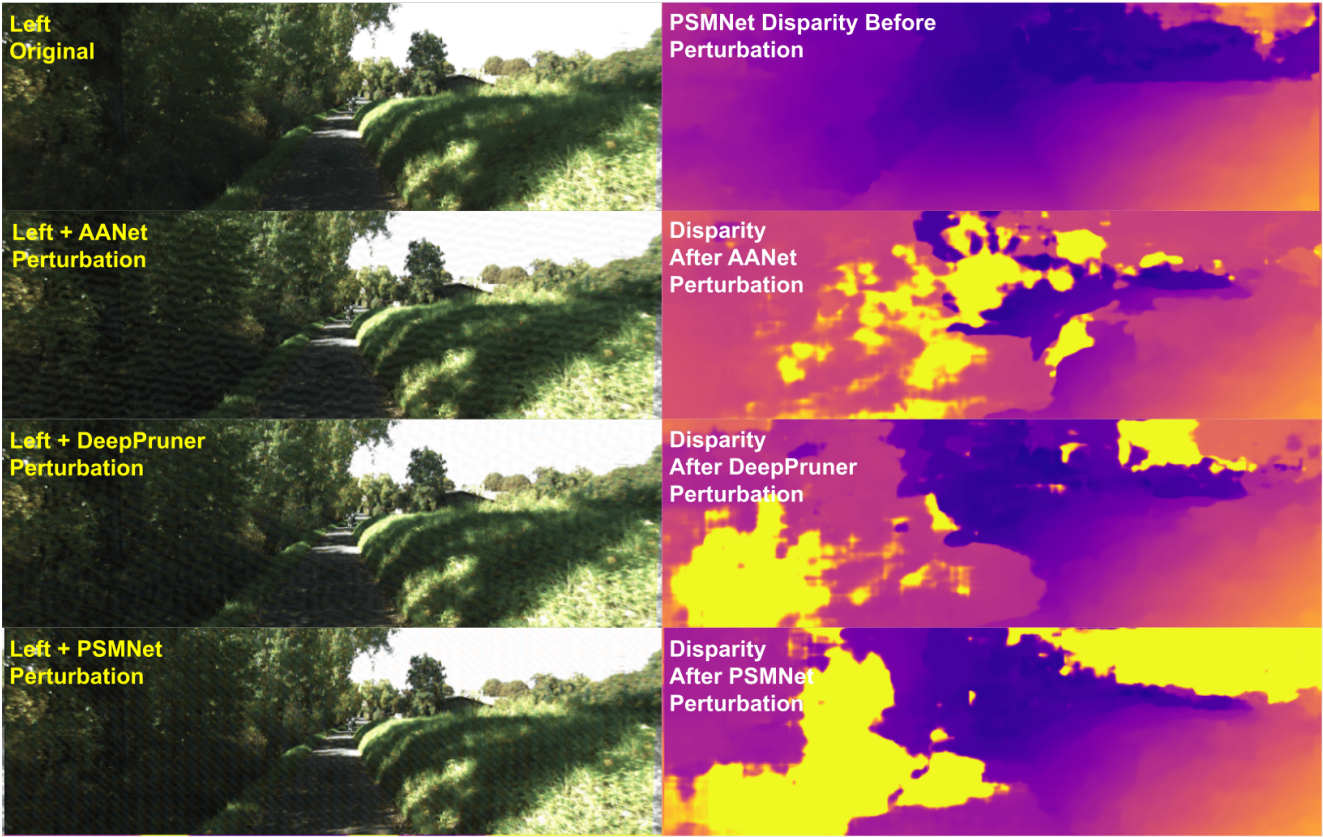


Figure 29. Attacking PSMNet for a scene from KITTI 2012 with a stereoscopic universal perturbations optimized on KITTI for AANet, DeepPruner, and PSMNet.

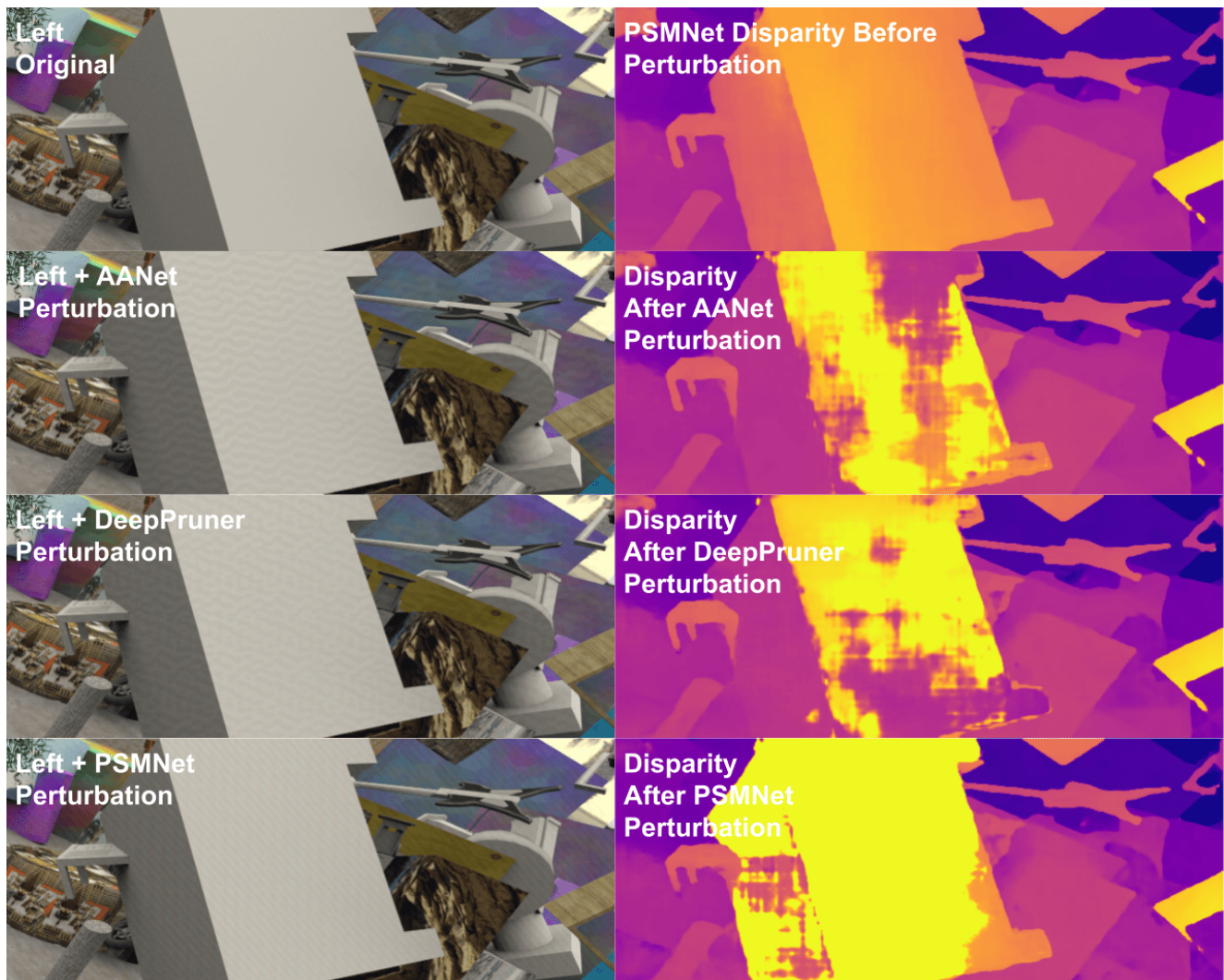


Figure 30. Attacking PSMNet for a scene from FlyingThings3D with a stereoscopic universal perturbations optimized on KITTI for AANet, DeepPruner, and PSMNet.